Virtual axis finder: a new method to determine the two kinematic axes of rotation for the tibio-femoral joint

by

Michelle Roland
B.S. (University of Colorado, Boulder) 2004

THESIS

Submitted in partial satisfaction of requirements for the degree of

MASTER OF SCIENCE

in

Biomedical Engineering

in the

OFFICE OF GRADUATE STUDIES

of the

UNIVERSITY OF CALIFORNIA

DAVIS

Approved

Maury L. Hull, Chair

David A. Hawkins

Benjamin J. Fregly

Committee in Charge

2010

ProQuest LLC
789 East Eisenhower Parkway
P.O. Box 1346
Ann Arbor, MI 48106-1346

ACKNOWLEDGMENTS

I would like to acknowledge Motion Analysis Corporation and Dustin Hatfield, as well as OtisMed Corporation for their support in our research program. I would like to thank my lab-mates, Esther Hodapp, Conrad Smith, and Deva Chan, for their continued support and advice throughout the progression of my research at UC Davis. I emphatically thank my major advisors, Maury L. Hull and Stephen M. Howell, for their advice, expertise, and patience. I could not have asked for better mentors. I acknowledge all of the undergraduate volunteers that provided hands on support for this research along the way; they were tremendously helpful. Thank you to my committee members, David A. Hawkins and Benjamin J. Fregly, for your expert advice. Finally, thank you to my loving parents, Laurie and Bernie Roland, as well as my sister, Hillary Roland, for their dedicated love and support throughout this process.

PREFACE

This thesis contains two chapters. The first chapter has been published in the Journal of Biomechanical Engineering in January 2010. The second Chapter will be submitted to the Journal of Biomechanical Engineering upon its completion. Thus, the structure of this thesis is such that each chapter is a stand-alone document.

CHAPTER 1
Derivation, validation and sensitivity analysis of the virtual axis finder

ABSTRACT

The tibio-femoral joint has been mechanically approximated with two fixed kinematic axes of rotation, the longitudinal rotational axis in the tibia (LR axis) and the flexion-extension axis in the femur (FE axis). The mechanical axis finder developed by Hollister et al. (1993) identified the two fixed axes but the visual-based alignment introduced errors in the method. Therefore, the objectives were to develop and validate a new axis finding method to identify the LR and FE axes which improves on the error of the mechanical axis finder. The virtual axis finder retained the concepts of the mechanical axis finder but utilized a mathematical optimization to identify the axes. Thus, the axes are identified in a two-step process: first, the LR axis is identified from pure internal-external rotation of the tibia and the FE axis is identified after the LR axis is known. The validation used virtual simulations of 3D video-based motion analysis to create relative motion between the femur and tibia during pure internal-external rotation, and flexion-extension with coupled internal-external rotation. The simulations modeled tibio-femoral joint kinematics and incorporated 1 mm of random measurement error. The root mean squared errors (RMSE) in identifying the position and orientation of the LR and FE axes with the virtual axis finder were 0.45 mm and 0.20°, and 0.11 mm and 0.20° respectively. These errors are at least 2 times better in position and 7 times better in orientation than those of the mechanical axis finder. Variables which were considered a potential source of variation between joints and/or measurement systems were tested for their sensitivity to the RMSE of identifying the axes. Changes in either the position or orientation of a rotational axis resulted in high sensitivity to position RMSE (6.8 mm of

RMSE per mm of translation) and orientation RMSE (1.38° of RMSE per ° of rotation) respectively. Notwithstanding these high sensitivities, corresponding errors can be reduced by segmenting the range of motion into regions where changes in either position or orientation are small. The virtual axis finder successfully increased the accuracy of the mechanical axis finder when the axes of motion are fixed with respect to the bones, but must be used judiciously in applications which do not have fixed axes of rotation.

INTRODUCTION

Modeling knee kinematics has been heavily studied in the biomechanics literature because it aids in clinical diagnostics [1-4], helps understand sport injury mechanisms [5, 6], and is essential in developing new joint prosthetics and arthroplasties [3, 7-9]. Furthermore, modeled kinematics have been shown to be sensitive to the selection of the rotational axes [10-14], so the position and orientation of joint rotational axes must be accurately determined to properly model joint kinematics. Accordingly, it is important to develop an accurate method of defining a rotational axis model under a variety of conditions.

Several methods for defining rotational axes have been described in the literature, however each has its limitations. One method for finding the axes is a mechanical axis finder, however there is an error of 1 mm in positioning and 1.5 degrees in orientation [15]. A second method used the compound hinge model [16], however the mathematical description of the technique was too limited to evaluate the reliability of the method. A third method found two rotational axes from coupled rotations in the ankle [4], but the technique has not been applied to the knee. While this technique accurately identifies the ankle's rotational axes, it requires at least 25˚ of rotation to occur about both axes

simultaneously, which is not applicable to the knee joint because of the limited internal-external rotation during bending. Thus, there remains a need for a quantitative and mathematically clear method of determining the two rotational axes in the tibio-femoral joint.

The application of the mechanical axis finder showed that de-coupling the flexion-extension and internal-external rotations of the knee joint during bending is a viable method of identifying and describing knee kinematics [15]. However, the major source of error in this technique was the visually-based alignment of the axis finder to the rotational axes. Thus, one objective was to render the axis finder concept more objective by creating a virtual axis finder that utilizes a mathematical optimization in conjunction with simulated experimental data which is representative of tibio-femoral kinematics reported in the literature to identify the FE and LR axes. By changing the implementation of the axis finder from being a visually-based procedure to being a mathematical optimization, our goal was to improve the error.

A second objective was to validate the virtual axis finder. A number of variables, such as random error in the kinematic data and range of internal-external rotation may differ between measurement modalities and/or condition of the knee. Because these variables can affect the accuracy of the method, it was of interest in the validation to conduct a sensitivity analysis for each variable using the bias, precision, and root mean square (RMS) of the error in locating the LR and FE axes as dependent variables.

METHODS

Although the validation of the method presented here was performed virtually, the method was developed to be applied specifically to a tibio-femoral joint. Therefore,

anatomic references and figures are used here to guide the application of this virtual validation to an actual tibio-femoral joint. All points, coordinate systems, and motions were created virtually such that they represented the anatomy and kinematics of an actual tibio-femoral joint.

The virtual axis finder mimics the methodology of the mechanical axis finder [15] by identifying the LR and FE axes in a two-step process. The first step identifies the LR axis from pure internal-external rotation of the tibia at several flexion angles. The second step identifies the FE axis from unconstrained flexion-extension with coupled internal-external rotation. Because the LR axis is already identified, the coupled internal-external rotation which occurs with flexion-extension can be mathematically eliminated.

To increase the accuracy over that of the mechanical axis finding method, the visual-based alignment of the mechanical pin to the axes was eliminated and replaced with a mathematical optimization. Thus, custom software was created which utilizes the input of 3D video-based motion analysis data of the internal-external rotation and unconstrained flexion-extension and outputs an optimized location of the axes (Figure 1.1).

To validate this custom software, simulated 3D video-based motion analysis data was created with a virtual two degree-of-freedom kinematic model of the tibio-femoral joint. The model consisted of two non-intersecting, perpendicular, fixed axes of rotation [15, 16] and a set of four markers fixed to each axis. Flexion-extension and internal-external rotations that were representative of tibio-femoral rotational kinematics reported in the literature were input into the model and the corresponding three-dimensional

positions of the markers rotating about the axes were output. Random measurement noise was added to the marker data to make it realistic.

The derivation of the mathematical optimization utilizes the following nomenclature: a position vector $\mathbf{r}$ expressed in coordinate system *a,* from point 1 (*p1*) fixed in one body to point 2 (*p2*) fixed in another body is expressed in Equation 1.1.

$$\mathbf{r_a^{p2/p1}} = x_a^{p2/p1}\hat{\mathbf{i}}_\mathbf{a} + y_a^{p2/p1}\hat{\mathbf{j}}_\mathbf{a} + z_a^{p2/p1}\hat{\mathbf{k}}_\mathbf{a} \qquad (1.1)$$

To describe the relative motion, two coordinate systems were established. The femoral anatomic coordinate system (F) was fixed in the femur. The origin was situated at the mid-point between the medial and lateral epicondylar eminences with $\hat{\mathbf{i}}_\mathbf{F}$ directed anteriorly, $\hat{\mathbf{j}}_\mathbf{F}$ directed medially, and $\hat{\mathbf{k}}_\mathbf{F}$ directed proximally. A similar anatomical coordinate system was fixed in the tibia (T) with the origin situated at the midpoint between the medial and lateral tibial eminences. Both coordinate systems were known at each instant in time in a global coordinate system (G).

Virtual Axis Finder

The virtual determination of the axes was based on the premise that a rotational axis can be defined by two points fixed in a rotating body which do not move with respect to the other body. Finding two points on the LR axis (*LR1* and *LR2*) required a non-linear optimization and an error function (*E)* which quantified the total relative motion between a point in the tibia (*l*) and the origin of the femoral anatomic coordinate system (*Fo*) (Equation 1.2). When any point on the LR axis is selected, E^{LR} goes to zero; therefore, Equation 2 was minimized two separate times in Matlab's non-linear least squares function to identify the coordinates of two points: *LR1* and *LR2* in T. Because there are an infinite number of points which exist along the rotational axis, the search

spaces for *LR1* and *LR2* were constrained to two parallel planes: the $\hat{\mathbf{i}}_T\hat{\mathbf{j}}_T$-plane approximately aligned with the tibial plateau ($z_T = 0$ cm), and the $\hat{\mathbf{i}}_T\hat{\mathbf{j}}_T$-plane 15 cm distal to the plateau ($z_T = -15$ cm), respectively. The total number of data points collected throughout internal-external rotation is represented by n, and the mean value of a variable for n data points is indicated with a bar.

$$E^{LR} = \sqrt{\frac{1}{n}\sum_{i=1}^{n}\left(\left(x_{F}^{l/Fo}{}_{i} - \bar{x}_F^{l/Fo}\right)^2 + \left(y_{F}^{l/Fo}{}_{i} - \bar{y}_F^{l/Fo}\right)^2\right)} \qquad (1.2)$$

The vector from *LR2* to *LR1* in T ($\mathbf{r}_{\mathbf{T}}^{\mathbf{LR1/LR2}}$) marked the position of the LR axis (Figure 1.2). The full derivation of the error function can be found in appendix A.

To identify the FE axis, two points fixed in the femur (*FE1* and *FE2*) which did not move with respect to the tibia had to be identified. However, it was not possible to search from any random point fixed in the tibia because of the natural internal-external rotation which occurs during flexion-extension [15-17]. To eliminate the movement of the selected point during the coupled rotations, the position vectors utilized in the error functions were from a point on the LR axis to two points fixed in the femur. Because the tibia's coordinate system rotates relative to the femur, the components of the vector are constantly shifting when a point on the FE axis is selected; however, the magnitude of the vector remains constant. Thus, the error function E^{FE} used to determine two points on the FE axis from natural flexion-extension coupled with internal-external rotations utilized the change in the magnitude of a vector from a point on the LR axis (*LR*) to a point (*f*) fixed in the femur (Equation 1.3). The search spaces for *FE1* and *FE2* were confined to

two parallel planes: the $\hat{\mathbf{i}}_F\hat{\mathbf{k}}_F$-plane containing the medial epicondylar eminence ($y_F = -5$ cm), and the $\hat{\mathbf{i}}_F\hat{\mathbf{k}}_F$-plane containing the lateral epicondylar eminence ($y_F = 5$ cm) respectively (Figure 1.3). Here, n indicates the total number of data points collected throughout flexion-extension.

$$E^{FE} = \sqrt{\frac{1}{n}\sum_{i=1}^{n}\left(\left|\mathbf{r}_{\mathbf{T}}^{\mathbf{f/LR}}\right|_i - \left|\bar{\mathbf{r}}_{\mathbf{T}}^{\mathbf{f/LR}}\right|\right)^2} \qquad (1.3)$$

The vector from the medial point on the FE axis (*FE1)* to the lateral point on the FE axis (*FE2)* in F ($\mathbf{r}_{\mathbf{F}}^{\mathbf{FE2/FE1}}$) marked the position of the FE axis. The full derivation of the error function is in appendix A.

Because $\mathbf{r}_{\mathbf{T}}^{\mathbf{LR1/LR2}}$ and $\mathbf{r}_{\mathbf{F}}^{\mathbf{FE2/FE1}}$ were described in anatomically relevant coordinate systems, the orientations of the axes were described with clinically relevant projection angles onto anatomical planes and the positions were described by coordinates of the intersection of the axis with the plane containing the coordinate system origin**.** The orientation of the LR axis was defined with the projection angle of $\mathbf{r}_{\mathbf{T}}^{\mathbf{LR1/LR2}}$ onto the $\hat{\mathbf{i}}_{\mathbf{T}}\hat{\mathbf{k}}_{\mathbf{T}}$-plane (FE orientation) and $\hat{\mathbf{j}}_{\mathbf{T}}\hat{\mathbf{k}}_{\mathbf{T}}$-plane (varus/valgus or VV orientation). The anterior-posterior ($x_T^{LR1/To}$) and medial-lateral ($y_T^{LR1/To}$) components of $\mathbf{r}_{\mathbf{T}}^{\mathbf{LR1/To}}$ defined the position of the LR axis. Similarly, the orientation of the FE axis was defined by the projection angle of $\mathbf{r}_{\mathbf{F}}^{\mathbf{FE1/FE2}}$ onto the $\hat{\mathbf{i}}_{\mathbf{F}}\hat{\mathbf{j}}_{\mathbf{F}}$-plane (IE orientation) and $\hat{\mathbf{i}}_{\mathbf{F}}\hat{\mathbf{k}}_{\mathbf{F}}$-plane (VV orientation). The point midway between FE1 and FE2 was utilized to describe the position of the FE axis because this point lies in the sagittal plane that contains the origin

of the femoral coordinate system. Therefore, the medial-lateral $\left(y_F^{\frac{(FE1+FE2)}{2}/Fo} \right)$ and proximal-distal $\left(z_F^{\frac{(FE1+FE2)}{2}/Fo} \right)$ components of the vector from *Fo* to the midway point $\left(\mathbf{r}_{\mathbf{F}}^{\frac{(\mathbf{FE1+FE2})}{\mathbf{2}}/\mathbf{Fo}} \right)$ defined the position of the FE axis. Thus, there were four clinically relevant dependent variables that described the orientation and position of each axis.

Validation

The virtual axis finder was validated with simulated kinematic data. The simulations were performed in Matlab 7.4.0. Initially, a simulation was performed on a baseline set of conditions which represented tibio-femoral kinematics that are reported in the literature. Several of these baseline conditions were selected for a sensitivity analysis because they are a potential source of variation, either from knee to knee, or from varying measurement modalities (Table 1.1).

Baseline Model

The simulations were created under the assumption that 3D video-based motion analysis was used for kinematic data collection. Two sets of four reflective markers were rigidly mounted to the femur and tibia. Each set of markers formed a Cartesian coordinate system with marker 1 defining the origin, marker 2 defining the x-axis, marker 3 defining the y-axis, and marker 4 defining the z-axis. Markers 2-4 were situated 5 cm from marker 1 along their respective axial directions.

The initial positions of the rotational axes were defined with respect to the global coordinate system. Two rotational axis coordinate systems were established: one in the

tibia (Ta) and one in the femur (Fa). The LR axis was defined as $\hat{\mathbf{k}}_{\mathbf{Ta}}$, $\hat{\mathbf{j}}_{\mathbf{Ta}}$ was oriented medially, and $\hat{\mathbf{i}}_{\mathbf{Ta}}$ was oriented anteriorly. The origin was situated on the mid-point between the medial and lateral tibial eminences. The FE axis was defined as $\hat{\mathbf{j}}_{\mathbf{Fa}}$, $\hat{\mathbf{i}}_{\mathbf{Fa}}$ was oriented anteriorly, and $\hat{\mathbf{k}}_{\mathbf{Fa}}$ was oriented proximally. The origin was situated at the center point between the medial and lateral epicondylar eminences. The LR axis was positioned perpendicular to the FE axis in the coronal plane but non-intersecting by 1 cm posterior [15, 16].

The tibial and femoral markers were virtually mounted with respect to the Ta and Fa coordinate systems respectively. Tibial marker 1 was positioned 10 cm distal and 5 cm medial from the tibial origin. Femoral marker 1 was positioned 15 cm proximal and 5 cm medial from the femoral origin.

The simulated data provided the motion of the two marker sets in the global coordinate system. A normally distributed random error term with zero mean was independently incorporated into each marker's data [18]. The precision was set conservatively to 1 mm [19, 20].

The range of motion that was simulated was selected from the literature. Pure internal-external rotation under a small applied torque (3 N-m) was simulated with 20 degrees of I-E rotation [21]. Natural flexion-extension was simulated with 90˚ of flexion and 15˚ internal rotation of the tibia which occurred during the first 30 degrees of flexion in a manner which emulated the screw home mechanism [16, 22, 23].

To verify that the global minimum was being determined with the optimization algorithm, a pilot study was performed in which the position of the LR axis was determined on the same set of internal-external rotational data for 100 iterations. For each

iteration, the error in the initial guess for the x_T and y_T components of *LR1* and *LR2* utilized in the optimization routine were independently randomized with a uniform random number generator (-20 mm to 20 mm). The standard deviations of the optimized position of *LR1* and *LR2* were determined to be 0.0010 mm and 0.0013 mm respectively. Thus, the optimization converged to the global minimum. Because the position of the initial guess was not a factor, the error in the initial guess was implemented as a random variable (σ^2= 10 mm, μ=0) throughout the validation.

Pilot studies revealed a large sensitivity to the random error in the marker positions. Therefore, rotational steps were simulated such that stepwise rotation was applied and held for a period of time. By averaging the position of the markers during each rotational step, the random error input into the software was filtered and the resulting error was greatly reduced. It was determined that both the number of rotational steps and the number of data points collected during each step reduced the error in finding the axes. The condition that was selected as the baseline condition for pure internal-external rotation of the tibia was 5 rotational steps (4° of rotation per step) with 500 data points per step (RMSE equal to 0.21º and 0.45 mm). The condition selected for natural flexion-extension of the tibia was 15 rotational steps (6° of rotation per step) with 500 data points collected per step (RMSE equal to 0.20º and 0.11 mm). These parameters were utilized because the RMSE values for the two motions were minimal and an increase in rotational steps did not provide a proportionate reduction in error. Furthermore, the parameters could be reasonably applied to the actual range of motions expected.

For each condition that was simulated, a new randomized data set and randomized initial guess were recreated for 100 iterations. An error (e_i) was determined for each result from

$$e_i = actual - measured_i \quad (4)$$

To quantify the accuracy of this method, the bias or average error, precision or random error, and root mean square error (RMSE) were determined over all 100 iterations within each test condition. The resulting error terms for the two projection angles were statistically pooled together to provide the overall orientation error, and the two position variables were statistically pooled together to provide the overall position error.

Test Conditions

Because the amount of random error in the kinematic data can vary from one system to the next [20], it was important to determine the sensitivity of the method to the random error. Therefore, the standard deviation of the random error term was varied from 0 mm to 10 mm in 1 mm increments to quantify the software's sensitivity to the random measurement error.

The amount of pure internal-external rotation of the tibia can vary greatly from knee to knee [21]. Therefore, it was important to understand how the range of motion (ROM) impacts the accuracy of this method. The error in finding the LR axis was determined from 5˚ to 45˚ of internal-external rotation in 5˚ increments.

Although this method assumes that the axes of rotation are fixed in the bone, this may not be a perfect assumption [16]. Therefore, it was important to quantify the error in determining the axis of rotation when an axis is not perfectly fixed in the bone. This was quantified under two separate conditions: translation and rotation of the LR axis. Pilot

studies revealed that the direction of translation and/or rotation did not affect the magnitude of the errors; therefore, only one position direction and one orientation direction were studied. To quantify the error from translating an axis of rotation, the instantaneous position of the LR axis was translated along the initial orientation of $\hat{\mathbf{i}}_{\mathbf{Ta}}$. The magnitude of the translation ranged from 0 mm to 20 mm of translation in 5 mm increments. To quantify the error from rotating the axis of rotation, the instantaneous orientation of the LR axis was rotated about the initial orientation of $\hat{\mathbf{i}}_{\mathbf{Ta}}$. The rotation of the axis' orientation ranged from 0˚ to 5˚of rotation in 1˚ increments. The translations and rotations of the LR axis were proportionately distributed throughout the 20˚ of internal-external rotation. The error term was calculated by subtracting the measured axis from the average position and orientation of the axis.

Because this method requires that the LR axis is determined before the FE axis can be determined, any error in the LR axis could be propagated when determining the FE axis. Therefore, the error in the FE axis was quantified after errors in the position of *LR1* were implemented. An error term was incorporated into the $x_T^{LR1/To}$ and $y_T^{LR1/To}$ components of the vector $\mathbf{r}_{\mathbf{T}}^{\mathbf{LR1/To}}$ in Equations A.13 and A.14, and the resulting error in the FE axis was quantified. The error term was varied from 0 mm to 20 mm in 5 mm increments.

RESULTS

The orientation and position RMSE for the orientation and position of the LR axis at the baseline conditions (Table 1.1) were 0.21˚ and 0.45 mm, respectively. The orientation and position RMSE of the orientation and position of the FE axis at the

baseline conditions (Table 1.1) with 90˚ flexion and 15˚ of coupled internal rotation were 0.20˚ and 0.11 mm, respectively.

Increasing the standard deviation of the random error term linearly increased the orientation and position RMSE of the orientation and position of the LR axis at a rate of 0.20º of RMSE per mm of random error (R^2=0.994) and 0.45 mm of RMSE per mm of random error (R^2=0.997), respectively. The precision increased at a similar rate while the bias was negligible (Figure 1.4).

The orientation and position RMSE of the LR axis decreased quadratically as the ROM increased. With 20˚ of rotation, the orientation and position RMSE dropped to 0.21˚ and 0.45 mm respectively. The bias was negligible (Figure 1.5).

Translating and rotating the axis of rotation throughout the 20˚ range of internal-external rotation caused the most drastic impact on the RMSE of the LR axis. Furthermore, it was the bias which predominantly caused the increase in RMSE rather than the precision. Translating the axis of rotation caused a linear increase in the position RMSE error at a rate of 6.8 mm of RMSE per mm of translation (R^2=0.998). The orientation RMSE remained constant at approximately 0.2˚ which is equivalent to the baseline error for the LR axis stated above; therefore, this error was considered negligible. Rotating the axis of rotation caused a linear increase in the orientation error at a rate of 1.38˚ of RMSE per degree of rotation (R^2=1). The position RMSE remained constant at approximately 0.4 mm which is equivalent to the baseline error stated above; therefore, this error was considered negligible (Figure 1.6).

The error in determining the FE axis which results from an input error in the position of *LR1* was relatively low. The orientation RMSE for determining the orientation of the FE

axis increased at a rate of 0.05 degrees of RMSE per mm of error in the position of *LR1* (R^2=0.971). The position RMSE was relatively constant at approximately 0.12 mm, which is nearly equivalent to the baseline error for the FE axis; therefore, this error was considered negligible (Figure 1.7).

DISCUSSION

Kinematic models of the tibio-femoral joint aid in clinical diagnostics, sport injury mechanisms, and the development of prosthetics and arthroplasties. Because the accurate identification of the rotational axes utilized in kinematic models can have a significant affect on their applicability, the objectives of this work were to develop and validate a method to determine the kinematic axes of rotation of the tibio-femoral joint. The virtual axis finder was developed such that it utilized the concepts of the mechanical axis finder [15] but eliminated the visual-based alignment method by implementing a mathematical optimization. The validation of the virtual axis finder provided several important indications of this method's capabilities. First, the errors in identifying the LR and FE axes of rotation with the virtual axis finder under parameters which represent expected physical conditions of a tibio-femoral joint were 0.20° and 0.45 mm, and 0.20° and 0.11 mm respectively. Second, the only variable which had a non-linear relationship with the RMSE was the range of internal-external rotation, which caused an exponential decrease in orientation and position RMSE as the range of rotation increased. However, even the highest errors reported with a small range of rotation were satisfactory. Finally, the translation and rotation of the LR axis had the largest linear sensitivities with the position and orientation RMSE respectively. Furthermore, the change in RMSE was

predominantly due to an increased bias rather than the precision. Thus, it is this variable which requires careful consideration.

There are several methods in the literature which identify the kinematic axes of the tibio-femoral joint [15, 16]. However, the only method which reports errors in a manner which is comparable to the baseline conditions examined here is the mechanical axis finder. Hollister et al. reported a 1 mm and 1.5° error in identifying a single axis of rotation [15]. Thus, the virtual axis finder reduced the error in identifying the orientation and position of a single axis of rotation by 55% and 86% respectively.

Because knee joints have varying internal-external rotational laxities [21], it is important that this method is capable of accurately identifying the LR axis from minimal amounts of internal-external rotation. At full extension, the range of pure internal-external rotation from a ± 3 Nm torque can be as low as 10° [21]. The results reported here indicate that with 10° of internal-external rotation, the orientation and position RMSE is 0.41° and 0.85 mm respectively, which is less than the errors reported for the mechanical axis finder [15]. Thus, the virtual axis finder will identify the LR axis more accurately than the mechanical axis finder despite the amount of internal-external rotational laxity of each individual tibio-femoral joint.

This method was developed on the assumption that the axes of rotation are fixed in the bone. Any translation and/or rotation of the rotational axis alters the motion of the markers in a plane perpendicular to the rotational axis, and consequently changes the apparent radius of curvature. This change in the radius of curvature causes the optimized center point of that motion to shift; resulting in a measurement bias. Hence, translation and rotation of the LR axis caused the greatest increase in the bias and RMSE of

identifying the LR axis. However, it is important to note that given a constant translation or rotation per degree of axial rotation, the RMSE of identifying an unfixed axis of rotation is smaller when there is a greater ROM. Thus, the virtual axis finder should be less sensitive to an unfixed FE axis of rotation than reported here for the LR axis because this degree of freedom has a larger ROM than internal-external rotation.

Because the assumption of fixed axes of rotation may not be valid for every application and because this method is sensitive to this assumption (Figure 1.6), it is important to have an alternative approach for applications which may not have fixed axes. The virtual axis finder had a lower RMSE for small ROM (Figure 1.5) than for unfixed axes (Figure 1.6); therefore, the total ROM can be shortened or partitioned until the assumption of fixed axes is valid within the partitioned ROM.

Another assumption used in this virtual validation concerns the orientation that was established between the bone coordinate systems (F and T) that were defined by the global position of the virtual markers and the coordinate systems utilized to establish the rotational axes (Fa and Ta). For simplicity, these two coordinate systems were aligned such that the defined rotational axes, FE and LR, were collinear with one of the axes of F and T, respectively. In practice, this will not be the case. Actual markers will not be fixed to the bones such that at least two markers are positioned directly on the rotational axis allowing the bone coordinate system to align with the rotational axis. It is possible that when the bone coordinate system is skewed from the orientation of the rotational axis, the virtual axis finder will not be able to optimize the location of the rotational axis with the same precision. However, if the bone coordinate system is redefined in an anatomically relevant manner such that one axis is approximately aligned with the

rotational axis, then errors introduced from skewing the bone coordinate system from the rotational axis can be reduced. Thus, three anatomic landmarks in each bone should be digitized with respect to the bone markers to define the appropriate transformation from the marker-based coordinate system to an anatomically-based coordinate system. To approximately align an axis in each bone with the corresponding rotational axes, the femoral coordinate system must be approximately aligned to the transepicondylar axis and the tibial coordinate system must be approximately aligned with the long axis of the tibia. Because these anatomic axes are approximately aligned with the FE and LR rotational axes respectively [15, 16], the potential error introduced from bone markers that are skewed with respect to the rotational axes will be reduced.

The use of rotational steps, which were statically held for a period of time at each angular position, introduces potential challenges for implementing this method. Because it is important that there is no motion during each rotational step, because the number of steps utilized increases the accuracy of this method, and because there is limited range of motion for pure internal-external rotations, this method may require equipment which can control the rotation of the specimens within 1°. Any motion which occurs during each step must be minimized and the rotation between each step should be proportionately spaced.

An important aspect of the virtual axis finder is the production of pure internal-external rotation of the tibia about its LR axis. Several methods can be used to accomplish this task in vivo and in vitro. Hollister et al. (1993) produced the internal-external rotational moment manually to identify the LR axis. The accurate determination of the LR axis from this method was verified by attaching diodes to the LR axis and

tracking their motion during unconstrained flexion-extension. Because the diodes traced concentric circles in a plane perpendicular to the FE axis, it was concluded that the LR axis was accurately identified from the manual rotation. Thus, manually applying an IE moment on the tibia should produce pure internal-external rotation about the LR axis with an accuracy which is similar to the results reported for the mechanical axis finder. However, this motion can be produced more precisely through the use of a load application system which can apply an internal-external torque that has an adjustable orientation with respect to the tibio-femoral joint [24-26]. If a rotational torque is applied perfectly about the LR axis of the tibia, then all anterior-posterior and medial-lateral coupled translations of the joint should go to zero. Thus, by adjusting the rotational axis of the machine with respect to the tibia until the coupled translations are minimized, pure internal-external rotation can be produced [24].

Although this validation simulated 3D video-based motion analysis as the measurement modality, the virtual axis finder can be utilized with any three-dimensional kinematic measurement modality. For instance, electromagnetic sensors, roentgen stereophotogrammetric analysis (RSA), and CAD model-based shape matching techniques all could be used to quantify the relative motion between the tibia and femur. Because this validation assumed the markers were rigidly fixed to the bones, it is important that the markers utilized in any application of this method are also rigidly fixed in the bone. Therefore, 3D video markers and/or electromagnetic markers are applicable primarily with cadaveric specimens. Shape matching and RSA, on the other hand, could be utilized in clinical studies.

The benefit of using 3D video markers or electromagnetic sensors is that they can be rigidly fixed to the bones of cadaveric specimens before any surgical alterations have been performed on the joint. This enables tests to be performed on healthy, intact specimens and those results compared to the same joint after an alteration to that joint has occurred. For instance, a new surgical alignment technique for total knee arthroplasty has recently been developed and utilized [27]. This technique attempts to restore the kinematic axes of the pre-arthritic tibio-femoral joint; however, there is no data to support this claim. The virtual axis finder could be utilized to determine how well this alignment goal is achieved in cadaveric specimens.

Many applications of the virtual axis finder are possible with kinematic data collected with CAD model-based shape matching techniques. This technique superimposes the two-dimensional shape of an implanted component on the two-dimensional shape of that component in two separate radiograph or fluoroscopic images [28-30]. By superimposing both images, the three-dimensional position of that component and/or bone can be reconstructed. Shape matching is commonly used to study the kinematics of total knee arthroplasties by shape matching the femoral and tibial components [28, 31, 32]. Because the virtual axis finder utilizes three points fixed in each bone to define two coordinate systems and ultimately quantify the relative motion between the bones, three identifiable points must be established in the femoral and tibial components [33, 34]. Thus the relative position and orientation between the femoral and tibial components can be determined at proportionate intervals throughout internal-external rotation, and unconstrained flexion to determine the rotational axes of a knee after a total knee arthroplasty has been performed. One application of the CAD model-

based shape matching technique and the virtual axis finder would be to compare the rotational axes of the two alignment methods available for total knee arthroplasty: traditional mechanical axis alignment [35, 36] and kinematic alignment [27]. Many patients have had bi-lateral TKA procedures: one knee with traditional mechanical axis alignment, and one knee with kinematic alignment. Therefore, the virtual axis finder could be utilized on both knees, and a comparison in the rotational axes between the two alignment methods could be obtained.

RSA also provides a unique set of applications with the virtual axis finder. This technique utilizes small tantalum markers which are rigidly inserted into bone to track the three-dimensional position of that bone from two simultaneous radiograph images [37]. If the beads were inserted into a patient during surgery, then post-operative rotational kinematics could be tracked with the virtual axis finder by radiographing the bones at proportionate intervals throughout the prescribed rotations. One application of RSA would be to measure the change in the rotational axes over time following an anterior cruciate ligament reconstruction. Because it has been determined that the anterior cruciate reconstructions can lengthen in the months following the reconstruction [38], this technique could be utilized to determine whether this lengthening affects the position and/or orientation of the rotational axes.

By employing the methods developed by the mechanical axis finder and implementing a mathematical optimization, the virtual axis finder has advanced tibio-femoral kinematic modeling which should prove useful in a variety of applications. The thorough validation of this method in a virtual setting with respect to a variety of factors reported here provides researchers with the ability to appropriately apply this method to

their specific applications. An application of interest to our research group is to use the virtual axis finder in a cadaveric study to quantify how well the kinematic axes are restored with total knee arthroplasty (TKA). We plan to perform this study and report on this in a subsequent paper. Because the virtual axis finder has the capability to quantify and compare the rotational kinematics under a variety of knee conditions and with a variety of measurement modalities, it can become a useful tool in the field of knee biomechanics.

APPENDIX

Derivation of the error functions for the virtual axis finder

The rotational and position information which converts a position vector expressed in coordinate system 1 to a vector expressed in a coordinate system 2 (Equation A.1) is denoted by the transformation matrix $[\mathbf{T}_{2/1}]$. The transformation matrix $[\mathbf{T}_{2/1}]$ is a 4x4 matrix which contains a 3x3 rotational matrix $[\mathbf{R}_{2/1}]$ and a 3x1 displacement vector $\mathbf{r}_2^{O_1/O_2}$ (Equation A.2).

$$\mathbf{r}_2 = [\mathbf{T}_{2/1}] \cdot \mathbf{r}_1 \tag{A.1}$$

$$[\mathbf{T}_{2/1}] = \begin{bmatrix} 1 & 0 & 0 & 0 \\ x_2^{O_1/O_2} & \hat{\mathbf{i}}_2 \cdot \hat{\mathbf{i}}_1 & \hat{\mathbf{i}}_2 \cdot \hat{\mathbf{j}}_1 & \hat{\mathbf{i}}_2 \cdot \hat{\mathbf{k}}_1 \\ y_2^{O_1/O_2} & \hat{\mathbf{j}}_2 \cdot \hat{\mathbf{i}}_1 & \hat{\mathbf{j}}_2 \cdot \hat{\mathbf{j}}_1 & \hat{\mathbf{j}}_2 \cdot \hat{\mathbf{k}}_1 \\ z_2^{O_1/O_2} & \hat{\mathbf{k}}_2 \cdot \hat{\mathbf{i}}_1 & \hat{\mathbf{k}}_2 \cdot \hat{\mathbf{j}}_1 & \hat{\mathbf{k}}_2 \cdot \hat{\mathbf{k}}_1 \end{bmatrix} \tag{A.2}$$

The transformation matrices $[\mathbf{T}_{F/G}]_t$ and $[\mathbf{T}_{T/G}]_t$ were defined by the kinematic data at each instant in time (*t*). The inverse matrix reverses the direction of the transformation (Equation A.3).

$$[\mathbf{T}_{2/1}] = [\mathbf{T}_{1/2}]^{-1} \tag{A.3}$$

Therefore, the relative position of the femur with respect to the tibia could be determined (Equation A.4).

$$[\mathbf{T}_{F/T}] = [\mathbf{T}_{F/G}] \cdot [\mathbf{T}_{T/G}]^{-1} \tag{A.4}$$

The position of the LR axis is defined by two points fixed with respect to T (equations A.5 and A.6).

$$\mathbf{r}_{\mathbf{T}}^{\mathbf{LR1/To}} = x_T^{LR1/To}\hat{\mathbf{i}}_{\mathbf{T}} + y_T^{LR1/To}\hat{\mathbf{j}}_{\mathbf{T}} + z_T^{LR1/To}\hat{\mathbf{k}}_{\mathbf{T}} \quad \textbf{(A.5)}$$

$$\mathbf{r}_{\mathbf{T}}^{\mathbf{LR2/To}} = x_T^{LR2/Ta}\hat{\mathbf{i}}_{\mathbf{T}} + y_T^{LR2/Ta}\hat{\mathbf{j}}_{\mathbf{T}} + z_T^{LR2/Ta}\hat{\mathbf{k}}_{\mathbf{T}} \quad \textbf{(A.6)}$$

Because it is the change in position of *LR1* and *LR2* with respect to the femur throughout internal-external rotation that must be minimized, the position vectors $\mathbf{r}_{\mathbf{T}}^{\mathbf{LR1/To}}$ and $\mathbf{r}_{\mathbf{T}}^{\mathbf{LR2/To}}$ must be transformed from coordinate system T to coordinate system F for each instant in time, *t* (Equations A.7 and A.8). The subscript, *t*, denotes that the variable changes with time.

$$\mathbf{r}_{\mathbf{F}}^{\mathbf{LR1/Fo}}{}_t = \left[\mathbf{T}_{\mathbf{F/T}}\right]_t \cdot \mathbf{r}_{\mathbf{T}}^{\mathbf{LR1/Fo}} = x_F^{LR1/Fo}{}_t\hat{\mathbf{i}}_{\mathbf{F}} + y_F^{LR1/Fo}{}_t\hat{\mathbf{j}}_{\mathbf{F}} + z_F^{LR1/Fo}{}_t\hat{\mathbf{k}}_{\mathbf{F}} \quad \textbf{(A.7)}$$

$$\mathbf{r}_{\mathbf{F}}^{\mathbf{LR2/Fo}}{}_t = \left[\mathbf{T}_{\mathbf{F/T}}\right]_t \cdot \mathbf{r}_{\mathbf{T}}^{\mathbf{LR1/Fo}} = x_F^{LR2/Fo}{}_t\hat{\mathbf{i}}_{\mathbf{F}} + y_F^{LR2/Fo}{}_t\hat{\mathbf{j}}_{\mathbf{Fa}} + z_F^{LR2/Fo}{}_t\hat{\mathbf{k}}_{\mathbf{F}} \quad \textbf{(A.8)}$$

LR1 and *LR2* are positioned on the longitudinal rotational axis when $\mathbf{r}_{\mathbf{F}}^{\mathbf{LR1/Fo}}{}_t$ and $\mathbf{r}_{\mathbf{F}}^{\mathbf{LR2/Fo}}{}_t$ do not change over time. Thus, $x_T^{LR1/To}$, $y_T^{LR1/To}$, $x_T^{LR2/To}$, and $y_T^{LR2/To}$ are iteratively adjusted until the change in $x_F^{LR1/Fo}{}_t$, $y_F^{LR1/Fo}{}_t$, $z_F^{LR1/Fo}{}_t$, $x_F^{LR2/Fo}{}_t$, $y_F^{LR2/Fo}{}_t$, and $z_F^{LR2/Fo}{}_t$ is minimized. The error functions, E^{LR1} and E^{LR2}, quantify the change in $\mathbf{r}_{\mathbf{Fa}}^{\mathbf{LR1/Fo}}{}_t$ and $\mathbf{r}_{\mathbf{Fa}}^{\mathbf{LR2/Fo}}{}_t$ over time as a root mean square error (Equations A.9 and A.10). Here, n indicates the total number of points collected during internal-external rotation.

$$E^{LR1} = \sqrt{\frac{1}{n}\sum_{i=1}^{n}\left(\left(x_F^{LR1/Fo}{}_i - \bar{x}_F^{LR1/Fo}\right)^2 + \left(y_F^{LR1/Fo}{}_i - \bar{y}_F^{LR1/Fo}\right)^2 + \left(z_F^{LR1/Fo}{}_i - \bar{z}_F^{LR1/Fo}\right)^2\right)} \quad \textbf{(A.9)}$$

$$E^{LR2} = \sqrt{\frac{1}{n}\sum_{i=1}^{n}\left(\left(x_F^{LR2/Fo}{}_i - \bar{x}_F^{LR2/Fo}\right)^2 + \left(y_F^{LR2/Fo}{}_i - \bar{y}_F^{LR2/Fo}\right)^2 + \left(z_F^{LR2/Fo}{}_i - \bar{z}_F^{LR2/Fo}\right)^2\right)} \quad \textbf{(A.10)}$$

Because $x_F^{LR1/Fo}{}_t$, $y_F^{LR1/Fo}{}_t$, and $z_F^{LR1/Fo}{}_t$ are each functions of $x_T^{LR1/To}$ and $y_T^{LR1/To}$, E^{LR1} is minimized by adjusting $x_T^{LR1/To}$ and $y_T^{LR1/To}$. Similarly, E^{LR2} is minimized by adjusting $x_T^{LR2/To}$ and $y_T^{LR2/To}$.

The position of the FE axis is defined by two points (*FE1* and *FE2*) which are fixed with respect to F (Equations A.11 and A.12).

$$\mathbf{r}_\mathbf{F}^{\mathbf{FE1/Fo}} = x_F^{FE1/Fo}\hat{\mathbf{i}}_\mathbf{F} + y_F^{FE1/Fo}\hat{\mathbf{j}}_\mathbf{F} + z_F^{FE1/Fo}\hat{\mathbf{k}}_\mathbf{F} \quad \textbf{(A.11)}$$

$$\mathbf{r}_\mathbf{F}^{\mathbf{FE2/Fo}} = x_F^{FE2/Fo}\hat{\mathbf{i}}_\mathbf{F} + y_F^{FE2/Fo}\hat{\mathbf{j}}_\mathbf{F} + z_F^{FE2/Fp}\hat{\mathbf{k}}_\mathbf{F} \quad \textbf{(A.12)}$$

Because it is the change in position of *FE1* and *FE2* with respect to the tibia throughout flexion-extension that must be minimized, the position vectors of *FE1* and *FE2* must be transformed from coordinate system F to coordinate system T for each instant in time, *t*. Furthermore, because of the coupled internal-external rotation, the position vectors must go from a point on the LR axis (*LR1*) to a point fixed in the femur (Equation A.13 and A.14).

$$\mathbf{r}_\mathbf{T}^{\mathbf{FE1/LR1}}{}_t = \left[\mathbf{T}_{\mathbf{T/F}}\right]_t \cdot \mathbf{r}_\mathbf{F}^{\mathbf{FE1/Fo}} - \mathbf{r}_\mathbf{T}^{\mathbf{LR1/To}} = x_T^{FE1/LR1}{}_t\hat{\mathbf{i}}_\mathbf{T} + y_T^{FE1/LR1}{}_t\hat{\mathbf{j}}_\mathbf{T} + z_T^{FE1/LR1}{}_t\hat{\mathbf{k}}_\mathbf{T} \quad \textbf{(A.13)}$$

$$\mathbf{r}_\mathbf{T}^{\mathbf{FE2/LR1}}{}_t = \left[\mathbf{Ta}_{\mathbf{T/F}}\right]_t \cdot \mathbf{r}_\mathbf{F}^{\mathbf{FE2/Fo}} - \mathbf{r}_\mathbf{T}^{\mathbf{LR1/To}} = x_T^{FE2/LR1}{}_t\hat{\mathbf{i}}_\mathbf{T} + y_T^{FE2/LR1}{}_t\hat{\mathbf{j}}_\mathbf{T} + z_T^{FE2/LR1}{}_t\hat{\mathbf{k}}_\mathbf{T} \quad \textbf{(A.14)}$$

For the case of coupled rotations, the components of the vectors expressed in the tibial coordinate system will continue to change even once a point on the rotational axis is

selected because the tibial coordinate system is rotating as well. Therefore, the magnitude of equations A.12 and A.13 must be used for the error function. Hence, *FE1* and *FE2* are positioned on the flexion-extension axis when the magnitudes of $\mathbf{r}_{\mathbf{T}}^{\mathbf{FE1/LR1}}{}_{t}$ and $\mathbf{r}_{\mathbf{T}}^{\mathbf{FE2/LR1}}{}_{t}$ do not change with time. Thus, $x_F^{FE1/Fo}$, $z_F^{FE1/Fo}$, $x_F^{FE2/Fo}$, and $z_F^{FE2/Fo}$ are iteratively adjusted until the change in $\left|\mathbf{r}_{\mathbf{T}}^{\mathbf{FE1/LR1}}\right|$ and $\left|\mathbf{r}_{\mathbf{T}}^{\mathbf{FE2/LR1}}\right|$ over time is minimized. The error functions E^{FE1} and E^{FE2} quantify the changes in $\left|\mathbf{r}_{\mathbf{T}}^{\mathbf{FE1/LR1}}\right|$ and $\left|\mathbf{r}_{\mathbf{T}}^{\mathbf{FE2/LR1}}\right|$ as a root mean square error (Equations A.15 and A.16). Here, n is the total number of data samples taken during flexion-extension of the tibia.

$$E^{FE1} = \sqrt{\frac{1}{n}\sum_{i=1}^{n}\left(\left|r_T^{FE1/LR1}\right|_i - \left|\bar{r}_T^{FE1/LR1}\right|\right)^2} \qquad \textbf{(A.15)}$$

$$E^{FE2} = \sqrt{\frac{1}{n}\sum_{i=1}^{n}\left(\left|r_T^{FE2/LR1}\right|_i - \left|\bar{r}_T^{FE2/LR1}\right|\right)^2} \qquad \textbf{(A.16)}$$

Thus, E^{FE1} is minimized by adjusting $x_F^{FE1/Fo}$ and $z_F^{FE1/Fo}$. Similarly, E^{FE2} is minimized by adjusting $x_F^{FE2/Fo}$ and $z_F^{FE2/Fo}$.

REFERENCES

[1] Hicks, J., Arnold, A., Anderson, F., Schwartz, M., and Delp, S., 2007, "The effect of excessive tibial torsion on the capacity of muscles to extend the hip and knee during single-limb stance," Gait Posture, 26(4), pp. 546-552.

[2] Van Gheluwe, B., Kirby, K. A., and Hagman, F., 2005, "Effects of simulated genu valgum and genu varum on ground reaction forces and subtalar joint function during gait," J. Am. Podiatr. Med. Assoc., 95(6), pp. 531-541.

[3] Fuchs, B., Kotajarvi, B. R., Kaufman, K. R., and Sim, F. H., 2003, "Functional outcome of patients with rotationplasty about the knee," Clin. Orth. Rel. Res.(415), pp. 52-58.

[4] Reinbolt, J. A., Haftka, R. T., Chmielewski, T. L., and Fregly, B. J., 2008, "A computational framework to predict post-treatment outcome for gait-related disorders," Med. Eng.g Phys., 30(4), pp. 434-443.

[5] Besier, T. F., Lloyd, D. G., Ackland, T. R., and Cochrane, J. L., 2001, "Anticipatory effects on knee joint loading during running and cutting maneuvers," Med. Sci. Sports. Exerc., 33(7), pp. 1176-1181.

[6] Besier, T. F., Lloyd, D. G., Cochrane, J. L., and Ackland, T. R., 2001, "External loading of the knee joint during running and cutting maneuvers," Med Sci Sports Exerc, 33(7), pp. 1168-1175.

[7] Asano, T., Akagi, M., and Nakamura, T., 2005, "The functional flexion-extension axis of the knee corresponds to the surgical epicondylar axis: in vivo analysis using a biplanar image-matching technique," J. Arthroplasty, 20(8), pp. 1060-1067.

[8] Edwards, M. L., 2000, "Below knee prosthetic socket designs and suspension systems," Phys. Med. Rehabil. Clin. N. Am., 11(3), pp. 585-593, vi.

[9] Incavo, S. J., Coughlin, K. M., Pappas, C., and Beynnon, B. D., 2003, "Anatomic rotational relationships of the proximal tibia, distal femur, and patella: implications for rotational alignment in total knee arthroplasty," J. Arthroplasty, 18(5), pp. 643-648.

[10] Most, E., Axe, J., Rubash, H., and Li, G., 2004, "Sensitivity of the knee joint kinematics calculation to selection of flexion axes," J. Biomech., 37(11), pp. 1743-1748.

[11] Besier, T. F., Sturnieks, D. L., Alderson, J. A., and Lloyd, D. G., 2003, "Repeatability of gait data using a functional hip joint centre and a mean helical knee axis," J. Biomech., 36(8), pp. 1159-1168.

[12] Lenz, N. M., Mane, A., Maletsky, L. P., and Morton, N. A., 2008, "The effects of femoral fixed body coordinate system definition on knee kinematic description," J. of Biomech. Eng., 130(2), p. 021014.

[13] Ramakrishnan, H. K., and Kadaba, M. P., 1991, "On the estimation of joint kinematics during gait," J. Biomech., 24(10), pp. 969-977.

[14] Rivest, L. P., 2005, "A correction for axis misalignment in the joint angle curves representing knee movement in gait analysis," J. Biomech., 38(8), pp. 1604-1611.

[15] Hollister, A. M., Jatana, S., Singh, A. K., Sullivan, W. W., and Lupichuk, A. G., 1993, "The axes of rotation of the knee," Clin. Orth. Rel. Res., (290), pp. 259-268.

[16] Churchill, D. L., Incavo, S. J., Johnson, C. C., and Beynnon, B. D., 1998, "The transepicondylar axis approximates the optimal flexion axis of the knee," Clin. Orth. Rel. Res., (356), pp. 111-118.

[17] Asano, T., Akagi, M., Tanaka, K., Tamura, J., and Nakamura, T., 2001, "In vivo three-dimensional knee kinematics using a biplanar image-matching technique," Clin. Orth. Rel. Res., (388), pp. 157-166.

[18] Sonka, M., Hlavac, V., and Boyle, B., 1999, Image Processing, Analysis, and Machine Vision, Brooks/Cole Publishing Company, Pacific Grove.

[19] DeLuzio, K. J., Wyss, U. P., Li, J., and Costigan, P. A., 1993, "A procedure to validate three-dimensional motion assessment systems," J. Biomech., 26(6), pp. 753-759.

[20] Windolf, M., Gotzen, N., and Morlock, M., 2008, "Systematic accuracy and precision analysis of video motion capturing systems - exemplified on the Vicon-460 system," J. Biomech., 41(12), pp. 2776-2780.

[21] Blankevoort, L., Huiskes, R., and de Lange, A., 1988, "The envelope of passive knee joint motion," J. Biomech., 21(9), pp. 705-720.

[22] Johal, P., Williams, A., Wragg, P., Hunt, D., and Gedroyc, W., 2005, "Tibio-femoral movement in the living knee. A study of weight bearing and non-weight bearing knee kinematics using 'interventional' MRI," J. Biomech., 38(2), pp. 269-276.

[23] Coughlin, K. M., Incavo, S. J., Churchill, D. L., and Beynnon, B. D., 2003, "Tibial axis and patellar position relative to the femoral epicondylar axis during squatting," J. Arthroplasty, 18(8), pp. 1048-1055.

[24] Bach, J. M., and Hull, M. L., 1995, "A new load application system for in vitro study of ligamentous injuries to the human knee joint," J. Biomech. Eng., 117(4), pp. 373-382.

[25] Martin, K. J., Neu, C. P., and Hull, M. L., 2007, "An MRI-based method to align the compressive loading axis for human cadaveric knees," J. Biomech. Eng., 129(6), pp. 855-862.

[26] Durselen, L., Claes, L., and Kiefer, H., 1995, "The influence of muscle forces and external loads on cruciate ligament strain," Am. J. Sports Med., 23(1), pp. 129-136.

[27] Howell, S. M., Kuznik, K., Hull, M. L., and Siston, R. A., 2008, "Results of an initial experience with custom-fit positioning total knee arthroplasty in a series of 48 patients," Orthopedics, 31(9), pp. 857-863.

[28] Banks, S., Bellemans, J., Nozaki, H., Whiteside, L. A., Harman, M., and Hodge, W. A., 2003, "Knee motions during maximum flexion in fixed and mobile-bearing arthroplasties," Clin. Orth. Rel. Res., (410), pp. 131-138.

[29] Bingham, J., and Li, G., 2006, "An optimized image matching method for determining in-vivo TKA kinematics with a dual-orthogonal fluoroscopic imaging system," J. Biomech.l Eng., 128(4), pp. 588-595.

[30] Fantozzi, S., Leardini, A., Banks, S. A., Marcacci, M., Giannini, S., and Catani, F., 2004, "Dynamic in-vivo tibio-femoral and bearing motions in mobile bearing knee arthroplasty," Knee Surg. Sports Traumatol. Arthrosc., 12(2), pp. 144-151.

[31] Mahoney, O. M., Kinsey, T. L., Banks, A. Z., and Banks, S. A., 2008, "Rotational Kinematics of a Modern Fixed-Bearing Posterior Stabilized Total Knee Arthroplasty," J. Aarthroplasty, 24(4), pp. 641-645.

[32] Moro-oka, T. A., Muenchinger, M., Canciani, J. P., and Banks, S. A., 2007, "Comparing in vivo kinematics of anterior cruciate-retaining and posterior cruciate-retaining total knee arthroplasty," Knee Surg. Sports Traumatol. Arthrosc., 15(1), pp. 93-99.

[33] Sato, T., Koga, Y., and Omori, G., 2004, "Three-dimensional lower extremity alignment assessment system: application to evaluation of component position after total knee arthroplasty," J. Arthroplasty, 19(5), pp. 620-628.

[34] Moro-oka, T. A., Hamai, S., Miura, H., Shimoto, T., Higaki, H., Fregly, B. J., Iwamoto, Y., and Banks, S. A., 2007, "Can magnetic resonance imaging-derived bone models be used for accurate motion measurement with single-plane three-dimensional shape registration?," J. Orthop. Res., 25(7), pp. 867-872.

[35] Krackow, K. A., Bayers-Thering, M., Phillips, M. J., and Mihalko, W. M., 1999, "A new technique for determining proper mechanical axis alignment during total knee arthroplasty: progress toward computer-assisted TKA," Orthopedics, 22(7), pp. 698-702.

[36] Jessup, D. E., Worland, R. L., Clelland, C., and Arredondo, J., 1997, "Restoration of limb alignment in total knee arthroplasty: evaluation and methods," J South Orthop Assoc, 6(1), pp. 37-47.

[37] Weidenhielm, L., Wykman, A., Lundberg, A., and Brostrom, L. A., 1993, "Knee motion after tibial osteotomy for arthrosis. Kinematic analysis of 7 patients," Acta Orthop Scand, 64(3), pp. 317-319.

[38] Khan, R., Konyves, A., Rama, K. R., Thomas, R., and Amis, A. A., 2006, "RSA can measure ACL graft stretching and migration: development of a new method," Clin Orthop Relat Res, 448, pp. 139-145.

TABLES

Table 1.1: The test variables and their ranges which were examined in the validation of the virtual axis finder.

Variable	Range	Increments	Baseline conditions
Standard deviation of random error	0 mm -10 mm	1 mm	1 mm
Range of internal-external motion	5˚- 45˚	5˚	20°
Translation of LR axis	0 mm - 20 mm	5 mm	0 mm
Rotation of LR axis	0˚-5˚	1˚	0°
Error in *LR1* ($x_T^{LR1/To}$, $y_T^{LR1/To}$)	(0 mm, 0 mm) - (20 mm, 20 mm)	(5 mm, 5 mm)	(0 mm, 0 mm)

FIGURES

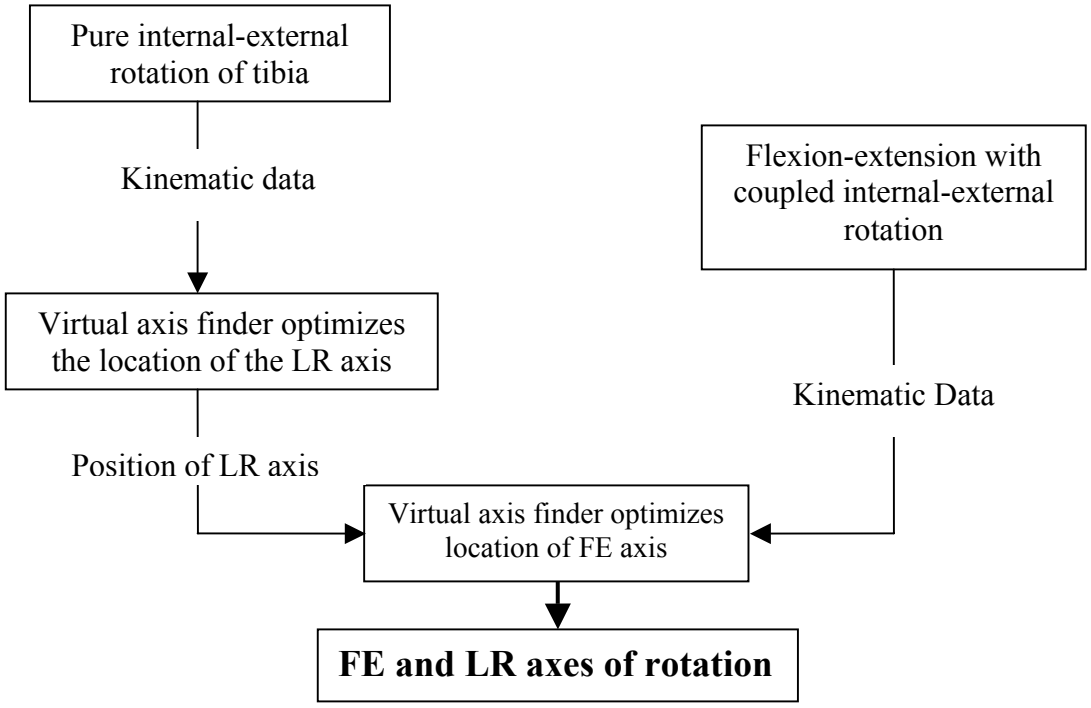

Figure 1.1: Flow chart representing the sequence of steps for the virtual axis finder.

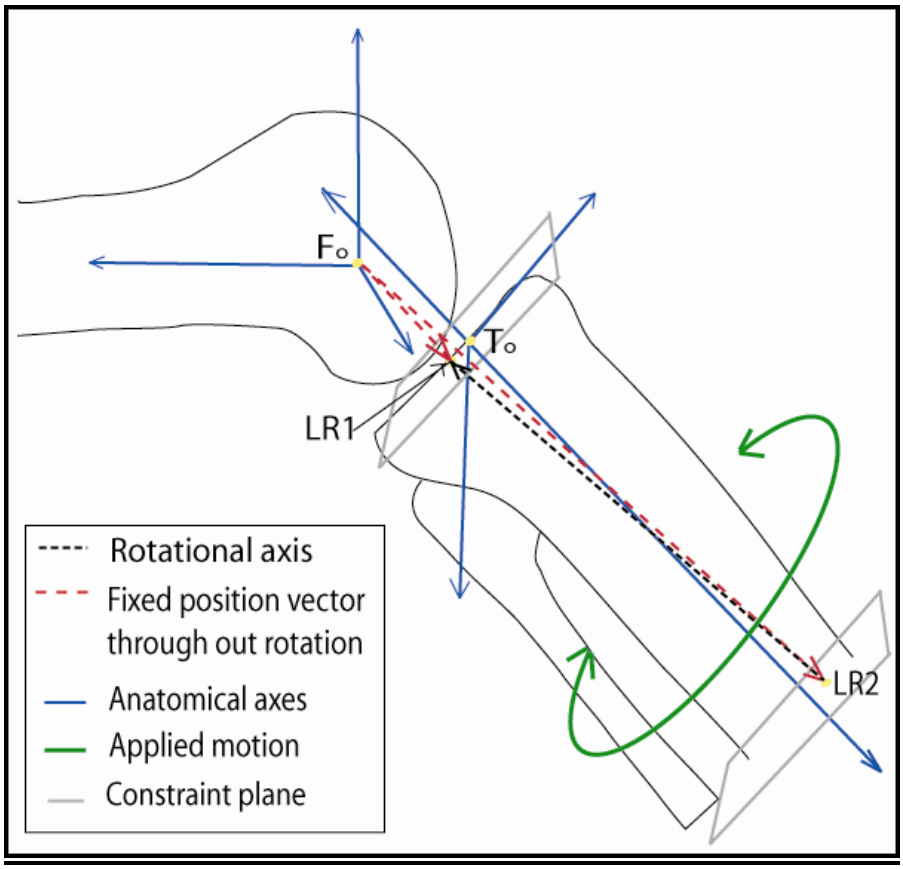

Figure 1.2: A schematic shows the coordinate systems used to determine the LR axis of rotation (line from LR1 to LR2). From the motion that resulted from an applied internal-external rotational moment on the tibia, two points (LR1, LR2) were identified in the tibia that did not move with respect to the femur: *LR1* is constrained to a plane in the tibia which was adjacent to the tibial plateau, and *LR2*, is constrained to a plane in the tibia distal to the tibial plateau. F_o is the origin of the femoral anatomic coordinate system which is fixed in the femur. T_o is the origin of the tibial anatomic coordinate system fixed in the tibia.

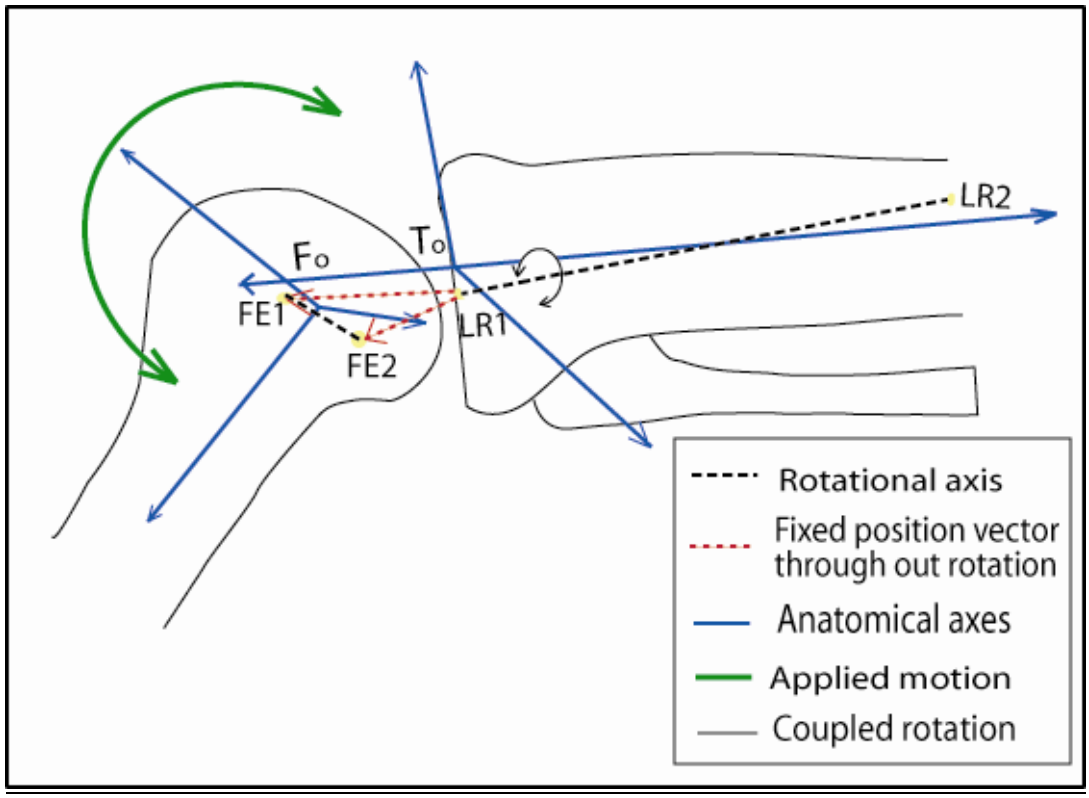

Figure 1.2: A schematic represents the coordinate systems used to determine the FE axis of rotation (line from FE1 to FE2). With an applied flexion-extension rotation of the femur, the tibia will naturally internally and externally rotate. Therefore, the search for two position vectors whose magnitudes do not change during the rotation was initialized from a point on the LR axis (*LR1*). The search for the first point, *FE1*, is constrained to a plane fixed in the femur which contains the medial epicondylar eminence. The search for the second point, *FE2*, is constrained to a plane fixed in the femur which contains the lateral epicondylar eminence. F_o is the origin of the femoral anatomic coordinate system which is fixed in the femur. T_o is the origin of the tibial anatomic coordinate system fixed in the tibia.

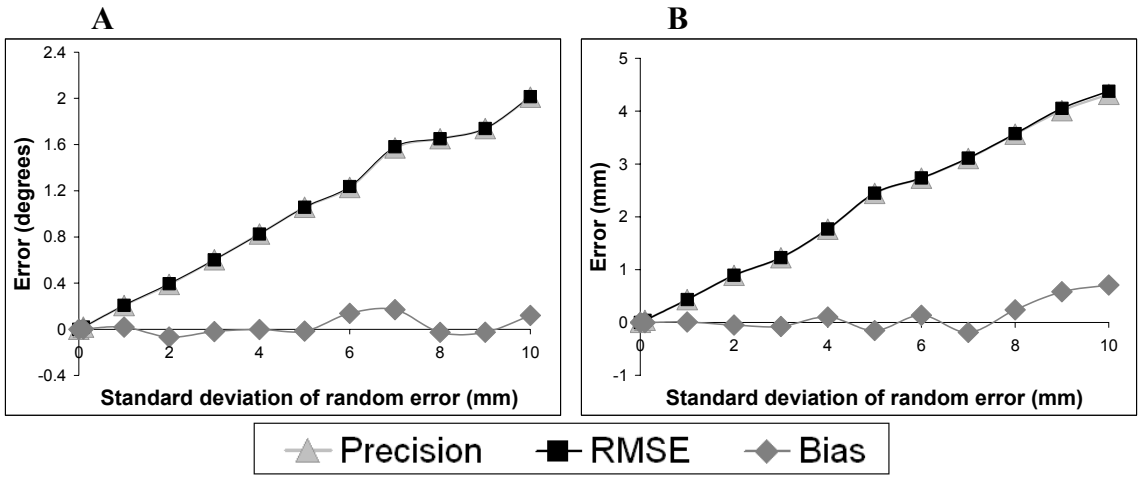

Figure 1.3: The RMSE, precision, and bias in determining the LR axis as the random measurement error increases. Figure A depicts the pooled orientation errors and Figure B depicts the pooled position errors. The orientation and position RMSE for the LR axis at the baseline condition of σ=1 mm was 0.21˚ and 0.45 mm respectively.

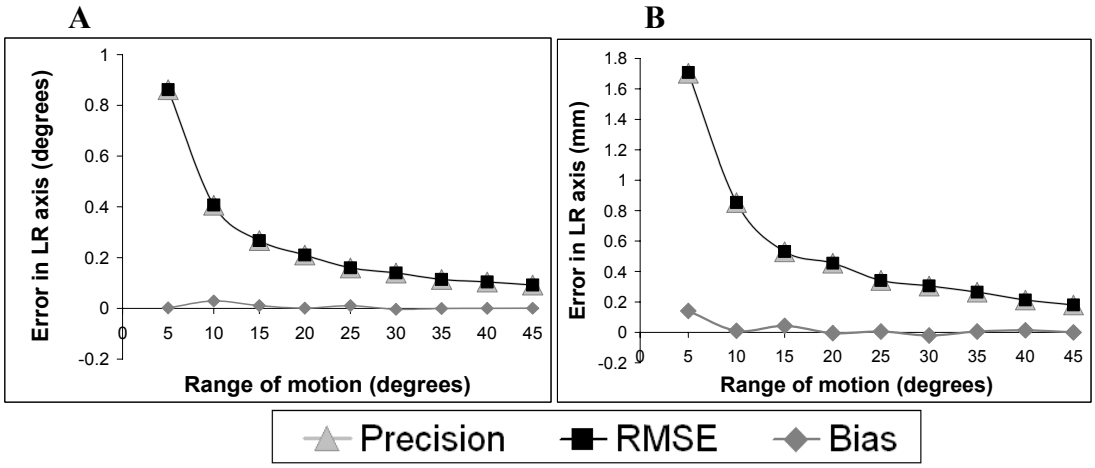

Figure 1.4: The RMSE, precision, and bias in identifying the LR axis which results from varying levels of internal-external tibial rotation. Figure A depicts the pooled orientation errors and Figure B depicts the pooled position errors. The orientation and position RMSE for the LR axis at the baseline condition of 20˚ was 0.21˚ and 0.45 mm respectively.

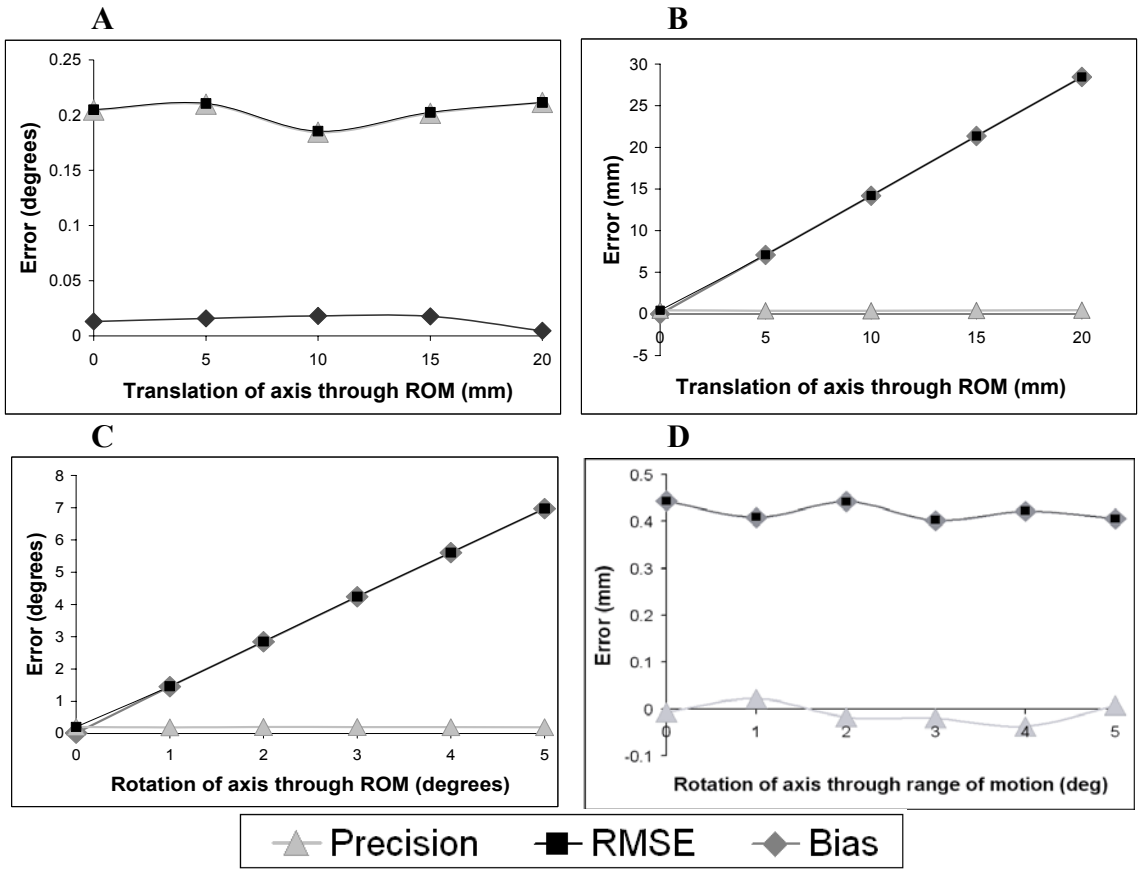

Figure 1.5: The RMSE, precision, and bias which results from determining the position of the LR axis when its position (A and B) or orientation (C and D) does not stay fixed. Figures A and C depict the pooled orientation error and B and D depict the pooled translation errors. Note that the RMSE in figures A and D are nearly equivalent to the baseline RMSE for the LR axis. Thus, the error is due to the random error term in the data rather than the translation and/or rotation of the LR axis.

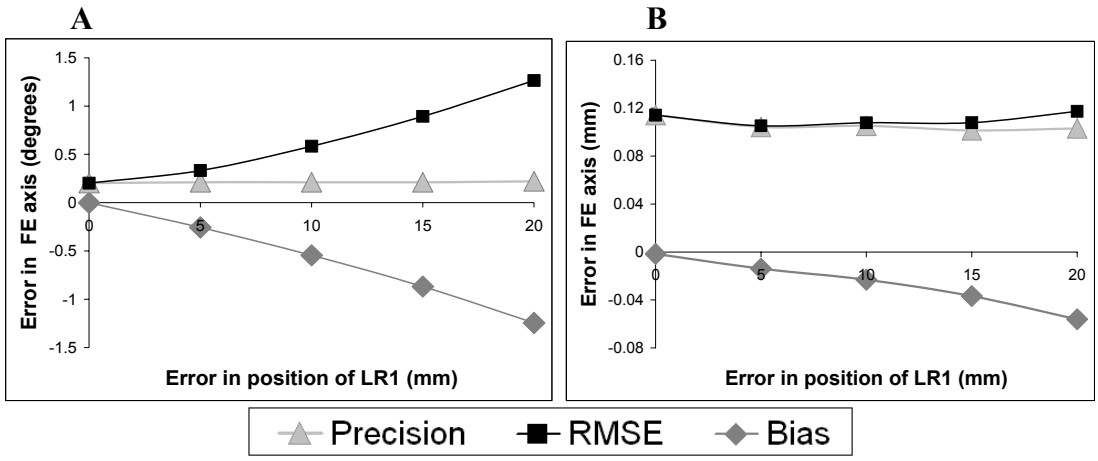

Figure 1.6: The RMSE, precision, and bias for determining the FE axis after an error in the position of *LR1* was incorporated into the optimization. Figure A depicts the pooled orientation errors and Figure B depicts the pooled position errors. Note that the non-zero orientation and position RMSE reported for 0 mm of input error in the position of *LR1* equates to the baseline error for determining the FE axis given 90˚ of flexion with 15˚ of internal rotation and a random error term (σ=1mm, μ=0).

CHAPTER 2
Error analysis of the virtual axis finder using both roentgen stereophotogrammetric analysis and 3D video-based motion analysis for kinematic measurements

ABSTRACT

In a previous paper, we reported the virtual axis finder, which is a new method for finding the rotational axes of the knee. The virtual axis finder was validated through simulations that were subject to limitations. Hence the objective of the present study was to perform a mechanical validation with two measurement modalities: 3D video-based motion analysis and roentgen stereophotogrammetric analysis (RSA). A two rotational axis mechanism was developed that simulated internal-external (or longitudinal) and flexion-extension rotations. The actual axes of rotation were known with respect to motion analysis and RSA markers within ±0.0006° and ±0.036 mm and ±0.0001° and ±0.016 mm, respectively. The orientation and position root mean squared errors (RMSEs) for identifying the longitudinal rotation (LR) and flexion-extension (FE) axes with motion analysis (0.26°, 0.28 mm, 0.36° and 0.25 mm, respectively) were smaller than with RSA (1.04°, 0.84 mm, 0.82° and 0.32 mm, respectively). The random error or precision in the orientation and position was significantly better (p=0.01 and p=0.02 respectively) in identifying the LR axis with motion analysis (0.23° and 0.24 mm) than with RSA (0.95° and 0.76 mm). There were no significant differences in the bias errors between measurement modalities. In comparing the mechanical validations to virtual validations, the virtual validations produced comparable errors to those of the mechanical validation. The only significant difference between the errors of the mechanical and virtual validations was the precision in the position of the LR axis while simulating motion analysis (0.24 and 0.78 mm, p=0.019). These results indicate that motion analysis

with the equipment used in this study is the superior measurement modality for use with the virtual axis finder, but both measurement modalities produce satisfactory results. The lack of significant differences between validation techniques suggests that the virtual sensitivity analysis previously performed was appropriately modeled. Thus, the virtual axis finder can be applied with a thorough understanding of its errors in a variety of test conditions.

INTRODUCTION

Identifying the rotational axes of the tibio-femoral joint and modeling knee kinematics have been heavily studied in the biomechanics literature because they aid in clinical diagnostics [1-4], help understand sport injury mechanisms [5, 6], and are essential in developing new joint prosthetics and arthroplasties [3, 7-9]. Several methods for identifying the rotational axes have been reported [10-12]; however each has its limitations. Recognizing these limitations motivated us to develop a new method called the virtual axis finder described in an earlier paper [12].

This virtual axis finder identifies the flexion-extension axis (FE axis) and the longitudinal rotational axis (LR axis) of the tibio-femoral joint by utilizing two mathematical optimizations given kinematic data from pure internal-external rotation and natural flexion-extension. This process is done in a two steps so that the coupled internal-external rotation that naturally occurs with flexion-extension can be mathematically eliminated when identifying the FE axis. The new method was validated virtually, with simulations of pure internal-external rotation and flexion-extension with coupled internal-external rotation. These simulations mimicked 3D video-based motion analysis as the kinematic measurement modality. The virtual validation included a sensitivity analysis,

which assessed the sensitivity of the method to several factors that may differ between specimens and/or measurement modalities.

The validation and sensitivity analysis of the virtual axis finder indicated a substantial reduction in error when compared to the other methods available, but several limitations motivate some additional development of the method. One is the lack of mechanical validation and the fact that the virtual validation simulated only one measurement modality. Another is that the virtual simulated kinematic data represented optimal data collection techniques and some variables, such as orientation of the axes with respect to the virtual markers and the lack of any measurement bias, were simplified in the virtual model. Furthermore, although this method might be applied with a variety of kinematic measurement modalities, only 3D video-based motion analysis was simulated.

These limitations to the previously reported validation necessitate a thorough mechanical validation in which the virtual axis finder is put into practice with multiple kinematic measurement modalities. Thus, the primary objective was to quantify and compare the bias, precision, and root mean squared error (RMSE) of the virtual axis finder with a mechanical knee simulator between two kinematic measurement modalities which can be used in vitro, bone mounted 3D video-based motion analysis and roentgen stereophotogrammetric analysis (RSA). As a secondary objective, the results of the mechanical validation were compared to virtual validations to assess the validity of the virtual simulations reported previously.

METHODS

Two Rotational Axis Mechanism

To validate mechanically the virtual axis finder, a mechanism that could produce two pure rotational motions about known axes of rotation had to be utilized. Thus, we developed a two rotational axis mechanism that simulated tibio-femoral flexion-extension and internal-external rotational kinematics (Figures 2.1 and 2.2). The mechanism allowed two rigid bodies to rotate independently about two fixed perpendicular axes of rotation [10,11]. The mechanism consisted of two shafts that were each supported by a pair of ball bearings and pillow blocks. To minimize off-axis motion of each shaft, we press fit the outer race of each ball bearing into custom made pillow blocks and the shafts were axially compressed against the inner race. The press fit and axial compression ensured that the axis of rotation for the shaft remained fixed with respect to the ball bearing and pillow block mechanism, which therefore allowed the geometrical axis of the shaft to remain collinear with the axis of rotation. To fix the two shafts with respect to one another, the two shafts and ball bearing pillow blocks were rigidly mounted to a base plate such that the axes of rotation were perpendicular and intersecting. Although the rotational axes may not be perpendicular and intersecting in practice, the relative position or orientation of the two rotational axes was examined virtually in pilot studies and no effect was observed. Precision-machined holes were placed on the pillow blocks in 5° increments about a 90° arc; this allowed the shafts to be rotated in 5° steps and pinned rigidly into place.

Because the objective was to simulate both RSA and 3D video-based motion analysis fixed to the bones, the two rotational axis mechanism was designed to be compatible with RSA tantalum markers as well as arrays of motion analysis reflective

markers (Figure 2.2). The position and orientation of both types of markers with respect to the axes of rotation were such that they simulated realistic placements in an actual tibio-femoral joint. Thus, the size, position, and orientation of the rotating shafts were selected to approximate the size and shape of a tibio-femoral joint truncated approximately 10-15 cm distal and proximal of the joint line. The longitudinal shaft simulated the tibia with six 0.8 mm tantalum markers fixed to the shaft such that they were equally spaced radially and axially about a 2.54 cm diameter and 10 cm length shaft, respectively. The horizontal shaft simulated the femur with six 0.8 mm tantalum markers fixed to a 5 cm x 8 cm plane approximately 8 cm from and parallel to the horizontal axis of rotation. The six markers were placed approximately 1 cm from one another within that plane. Although it only requires three markers to track the position and orientation of each shaft, six markers were used to over determine the system and aid in reducing the measurement error [13]. An array of four 1.90 cm diameter reflective markers was fixed to a rod that was inserted axially but off-center, and distally into the longitudinal shaft. A second array of four 1.90 cm diameter reflective markers was fixed to a rod that was inserted perpendicularly and proximal to the horizontal axis of rotation (Figure 2.1). The use of four-marker arrays over determined the system and aided in reducing the measurement error from motion analysis [13].

Gold Standard

To validate the virtual axis finder using the two rotational axis mechanism, the actual axes of rotation were identified with respect to the RSA markers and with respect to the motion analysis markers. For both cases, it was assumed that the geometric axes of the shafts were collinear with the axes about which the markers rotated. The axes were

identified with RSA by fixing RSA axial markers directly on the geometric axis of the shafts. Using a lathe (± 0.0125 mm), 0.8 mm diameter holes were drilled approximately 2.5 mm deep along the geometric axis from both ends. The size of the drill bit was selected such that the 0.8 mm tantalum marker could be inserted into the hole with minimum pressure but could not slide in without an applied force. To ensure that the holes were placed precisely along the axis of the shafts, the axial alignment of the shafts with the drilling axis of the lathe was verified with a dial indicator to have less than 0.025 ± 0.0125 mm of off-axis travel over the 10 cm length of the shaft (less than 0.01° angular error). One 0.8 mm tantalum marker was fixed into each hole to mark two points on each axis of rotation. A Monte Carlo simulation was performed to estimate the precision in identifying the orientation and position of the actual axes of rotation with respect to the RSA markers. Normally distributed random variables with a zero mean and standard deviation (σ) were input into the simulation. The machining precision (σ=0.025 mm) and the measurement precision of RSA (σ=0.05 mm) were randomized with a normal distribution 1,000 times and propagated through the calculations to identify the orientation and position errors of the actual axis with respect to the RSA markers. The output of the simulation estimated the precision of the orientation and position to be within ±0.0006° and ±0.036 mm, respectively.

The actual axes of rotation with respect to the motion analysis marker arrays were measured with a coordinate measurement machine (Model SLCHM005L, Mitutoyo Corp., Aurora, IL). The centroid of each marker was identified with a 15 point sphere identification algorithm. A point on the axis of the shafts and the unit vector along the axis of the shafts were identified with a 30 point cylinder identification algorithm.

Although the coordinate measurement machine has a 0.0001 mm precision, the irregularity of the reflective marker surfaces combined with the potential compliance of the arrays induced variability in identifying the centroids of the spheres and cylindrical axes. A truss system was added to each array to minimize the compliancy of the structure. To minimize the variability due to the irregularity of the marker surfaces, we increased the number of points used for each algorithm until the repeatability was equal to or less than 0.01 mm for the coordinates of each centroid and 0.0001 mm for the coordinates of the axial unit vector. A Monte Carlo simulation was performed to estimate the precision in identifying the orientation and position of the actual axes of rotation with respect to the motion analysis markers. Normally distributed random variables with a zero mean and standard deviation (σ) were input into the simulation. The repeatability in measuring the centroids of the markers (σ=0.01 mm) and the unit vector along the axis of the shaft (σ=0.0001 mm) were randomized 1,000 times with a normal distribution and propagated through the calculations to identify the orientation and position errors of the actual axis with respect to the motion analysis markers. The output of the simulation estimated the precision of the orientation and position to be within ±0.0001° and ±0.016 mm, respectively.

Testing

Global positions of the tantalum markers (± 0.05 mm) were obtained for each rotational step with bi-planar radiographs taken of the two rotational axis mechanism while it was positioned inside the RSA calibration cube. To simulate pure internal-external rotation, the longitudinal shaft was rotated in 5° increments from 0-20° while the horizontal shaft remained fixed at 30°. For flexion-extension with coupled internal-

external rotation, the horizontal shaft was rotated in 15° increments from 0-90° while the longitudinal shaft was rotated 15° during the first 30° of flexion. This process was repeated 5 times with the two rotational axis mechanism placed at various locations and orientations within the calibration cube to simulate 5 different specimens.

The motion analysis equipment and settings were utilized such that the tracking capabilities of the video cameras were optimized while maintaining a realistic laboratory setting for an in vitro study. Four 4.06 mega-pixel cameras (Raptor-4, Motion Analysis Corp, Santa Rosa, CA) were distributed evenly in a 1.5 m arc around a 0.6 m x 0.9 m x 0.6 m (l x w x h) calibrated volume. The cameras were vertically positioned between 1 m and 1.5 m above the base of the calibrated volume (Figure 2.3). Data were collected in grey scale mode at 100 Hz for 5 seconds per rotational step in the same sequence used for the RSA testing. The process was repeated 5 times with the two rotational axis mechanism in varying positions and orientations within the calibrated volume to simulate 5 different specimens. Before each specimen's data sets began, it was verified that no significant marker occlusions existed for all four cameras for the given orientation and position of the mechanism. The position vectors of all eight markers were averaged over the 5 second data set for each rotational step and the average vectors were input into the virtual axis finding software. Thus, RSA and motion analysis had the same number of rotational steps and the same range of motion input into the software for optimization of the rotational axes.

Data Analysis

To optimize the position and orientation of the longitudinal rotational axis (LR axis) and the horizontal rotational axis (FE axis), the virtual axis finding software was

utilized [12]. A marker coordinate system was defined and fixed to both the longitudinal (Tm) and horizontal (Fm) shafts. These coordinate systems were defined by three of the markers that were rigidly fixed to each shaft. To ensure that the constraint planes used to optimize the location of two points on each axis of rotation were approximately perpendicular to the axis of rotation, we had to transform the marker coordinate systems such that they were aligned with the axes of rotation. A pilot study was performed to ensure that deviating from this condition up to 5° and up to 5 mm does not affect the errors in this method. Thus, in practice, aligning the LR axis with the anatomic axis of the tibia and the FE axis with the transepicondylar axis of each coordinate system can create this transformation [10, 11]. However, for this application, the marker coordinate systems, Tm and Fm, were transformed into axial coordinate systems, Ta and Fa, such that an axis in each of the axial coordinate systems was aligned with the LR axis and FE axis, respectively. Because the actual axes of rotation were collinear with one axis of their respective coordinate systems that were used to quantify the error, two projection angles fully described the error in orientation (Figure 2.4). The position error was defined as the 2D position vector from the actual axes of rotation to the measured axes of rotation in a plane perpendicular to the actual LR ad FE axes. Because there are an infinite number of planes perpendicular to these axes, the plane with the smallest position vector magnitude was used to avoid compounding orientation error into the position error. Thus, the error for each axis of rotation was described with four dependent variables: two orientation variables and two position variables (Figure 2.4).

To quantify the accuracy of this method, we determined the bias defined as the average error, precision or random error defined as the standard deviation of the error,

and root mean square error (RMSE) over all 5 specimens and each dependent variable. The resulting error terms for the two projection angles were statistically pooled to provide the overall orientation error, and the two position variables were statistically pooled to provide the overall position error.

In the previous paper [12], a more thorough sensitivity analysis was performed in the virtual simulations; however, because these simulations were performed virtually, their applicability may be limited due to the assumptions and simplifications utilized in the virtual model. Thus, a comparison between the virtual validation and mechanical validation results was performed. Although the 3D video-based motion analysis virtual simulations were reported in the previous paper, certain aspects of that simulation did not correspond to the two rotational axis mechanism. Thus, the virtual validation was repeated such that marker positioning, measurement error, and positional error definitions aligned with the mechanical validation reported here. Virtual simulations of the RSA measurement modality were also performed as a second comparison of the two validation techniques. The RSA virtual model placed the markers in similar locations with respect to one another and to the axes as they were in the two rotational axis mechanism, and a measurement error of 0.05 mm [14] was incorporated into the virtual data. The virtual validation with motion analysis and RSA were each repeated 1,000 times with re-randomized data to estimate the error accurately.

The variances between RSA and motion analysis for the orientation and position errors for the LR and FE axes were subjected to an F-test for variances (α=0.05) to determine whether there was a significant difference in the precision of identifying the axes between measurement modalities. Similarly, the variances between mechanical and

virtual validations were subjected to an F-test (α=0.05) to determine whether there was a significant difference in the precision estimated from a mechanical validation versus a virtual validation. The mean error for each test was subjected to a student t-test (α=0.05) to determine whether there was a significant difference between measurement biases between measurement modalities as well as validation techniques. Independent two-sample t-tests for equal and unequal variances were utilized for each pair depending on the result of the F-test for equal variances. Finally, the MSE ratio between RSA and motion analysis measurement modalities was subjected to an F-test to determine if there were significant differences between measurement modalities with the RMSE.

RESULTS

The orientation and position errors for the LR and FE axes were considerably less with 3D video-based motion analysis than with RSA. The RMSEs in identifying the orientation and position of the LR axis with 3D video-based motion analysis were 0.26° and 0.28 mm, respectively, compared to 1.04° and 0.84 mm, respectively, with RSA. The orientation and position RMSE were 75% and 67% less with motion analysis than with RSA (Figure 2.5), which was a significant difference (p=0.01 and p=0.03, respectively). Likewise the RMSEs in identifying the orientation and position of the FE axis with 3D video-based motion analysis were 0.36° and 0.25 mm, respectively, compared to 0.82° and 0.32 mm, respectively, with RSA. The 56% decrease in orientation and 23% decrease in position RMSE with motion analysis compared to RSA with the FE axis was not significant (p=0.22 and p=0.41, respectively) (Figure 2.6).

There was significantly more variability (i.e. less precision) in identifying the orientation (p=0.008) and position (p=0.024) of the LR axis with RSA (0.95° and 0.76

mm) than with motion analysis (0.23° and 0.24 mm) (Figure 2.5). However, there were no significant differences between variances for the FE axis (p=0.07). Also there were no significant differences between bias errors for either the LR or FE axes (p=0.51).

In comparing the virtual validation to the mechanical validation, in general the errors compared closely for both motion analysis (TABLES

Table **2**.1) and RSA (Table 2.2). There was a significant difference between variances for the position errors (p=0.019) on the LR axis with motion analysis simulations; however, there were no other significant differences between validation techniques. The bias errors for the mechanical validations were non-zero whereas the bias errors for the virtual validation were negligible.

DISCUSSION

Identifying the rotational axes of the tibio-femoral joint and modeling knee kinematics have been heavily studied in the biomechanics literature, and the accuracy of these models have been shown to have a significant impact on their applicability. Limitations to previously reported methods to identify the rotational axes of the tibio-femoral joint prompted us to develop the virtual axis finder described in a previous paper [12]. However, there were several limitations to the virtual validation that necessitated a thorough mechanical validation in which the virtual axis finder was put into practice with multiple kinematic measurement modalities. Thus, our primary objective of this work was to validate mechanically the virtual axis finder with RSA and video-based motion analysis. A secondary objective was to compare the results of the mechanical validation to the virtual validations to verify the applicability of the previously reported virtual

validation. One key finding was that the errors for orientation and position of the LR and FE axes were reduced with motion analysis compared to RSA (Figures 2.5 and 2.6). A second key finding was that the validation performed with virtually created data produced higher errors than the validation performed with the two rotational axis mechanism. However, the difference in the precision of identifying the position of the LR axis while simulating motion analysis was the only dependent variable that was significantly different between validation techniques.

The fact that the precision in identifying the LR axis was significantly better with motion analysis than with RSA can be explained by two variables: the difference in measurement errors between the two measurement modalities and the use of multiple data points per rotational step with motion analysis. Although the exact measurement error of the motion analysis system used herein has not been reported, another four-camera Vicon system of similar capabilities was reported to have an overall measurement bias of 63 ± 5 μm and a measurement precision of 15 μm [20] in comparison to RSA which has negligible measurement bias and a measurement precision of 49 μm [14]. Furthermore, because RSA utilized just one set of radiographs at each rotational step, only one datum sample was available. On the other hand, motion analysis was collected at 60 Hz over 5 seconds providing 300 data samples per rotational step. Thus, utilizing the average result from a set of data provided improved measurement precision of the motion analysis data.

It is important to note that although the measurement precision of our data within a given rotational step and therefore given orientation of the markers was 6 μm and therefore comparable to the values reported with the Vicon system, an imprecision in the

distance between markers on the two arrays when the orientation of the arrays was changed was observed to be 150 μm. This imprecision was likely due to partial occlusions of the markers from the truss system built into the arrays for rigidity. Although this phenomenon did not have a large impact on the capabilities of the virtual axis finder, as evidenced by the results reported here, this phenomenon should be taken into consideration when designing motion analysis arrays in practice.

Because the virtual errors were consistently larger than the mechanical validation errors and because there were few significant differences between the mechanical and virtual validation techniques, it can be concluded that the virtual simulations appropriately modeled each measurement modality. This result provides evidence that the virtually-based sensitivity analysis reported previously is an accurate representation of the errors that can be expected in practice in the absence of skin movement artifacts. Furthermore, those results are, if anything, slightly over-estimating the errors.

An important assumption in this validation for video-based motion analysis as the measurement modality was the absence of skin motion artifact. It is our intention to use this method in a cadaveric study in which the marker arrays are fixed to the bones, thus eliminating skin motion artifact from this measurement modality. The application of this modality in vivo would undoubtedly introduce skin motion errors and deviate from the conditions tested here; therefore this modality should not be used with in vivo applications with further development to address these errors. However, because the measurement errors innate to RSA are not affected by in vivo applications, RSA could be used when this method is applied in vivo.

Another limitation with both the virtual and mechanical validation techniques was that the marker coordinate systems were fixed to the rotating bodies such that they were intentionally aligned to the actual axes of rotation. This was done to simplify the modeling and to provide anatomically relevant results. However, this was considered to be a potential source of error in practice because perfect alignment will not be possible. Thus, pilot studies were performed with the mechanical data in which the marker coordinate systems were translated and rotated from the actual axes of rotation. There were no changes to either the bias or the precision errors of the virtual axis finder during these pilot studies; therefore this independent variable and the attendant errors were not included in the analysis reported here.

The results of these validations indicate that 3D video-based motion analysis using four Raptor 4 cameras is a better measurement modality than RSA for use with the virtual axis finder; however, both methods provided satisfactory results. Given these results, the virtual axis finder maintains a large scope of applicability in the biomechanics field as suggested in the previous paper. Furthermore, because the virtual validation tends to over-estimate the error when compared to the mechanical validation, the sensitivity analysis reported previously estimates the upper end of the error scale with this method. Thus, this method can be utilized with a thorough understanding of the expected errors under a variety of test conditions and applications.

REFERENCES

[1] Hicks, J., Arnold, A., Anderson, F., Schwartz, M., and Delp, S., 2007, "The effect of excessive tibial torsion on the capacity of muscles to extend the hip and knee during single-limb stance," Gait Posture, 26(4), pp. 546-552.

[2] Van Gheluwe, B., Kirby, K. A., and Hagman, F., 2005, "Effects of simulated genu valgum and genu varum on ground reaction forces and subtalar joint function during gait," J. Am. Podiatr. Med. Assoc., 95(6), pp. 531-541.

[3] Fuchs, B., Kotajarvi, B. R., Kaufman, K. R., and Sim, F. H., 2003, "Functional outcome of patients with rotationplasty about the knee," Clin. Orth. Rel. Res.(415), pp. 52-58.

[4] Reinbolt, J. A., Haftka, R. T., Chmielewski, T. L., and Fregly, B. J., 2008, "A computational framework to predict post-treatment outcome for gait-related disorders," Med. Eng.g Phys., 30(4), pp. 434-443.

[5] Besier, T. F., Lloyd, D. G., Ackland, T. R., and Cochrane, J. L., 2001, "Anticipatory effects on knee joint loading during running and cutting maneuvers," Med. Sci. Sports. Exerc., 33(7), pp. 1176-1181.

[6] Besier, T. F., Lloyd, D. G., Cochrane, J. L., and Ackland, T. R., 2001, "External loading of the knee joint during running and cutting maneuvers," Med Sci Sports Exerc, 33(7), pp. 1168-1175.

[7] Asano, T., Akagi, M., and Nakamura, T., 2005, "The functional flexion-extension axis of the knee corresponds to the surgical epicondylar axis: in vivo analysis using a biplanar image-matching technique," J. Arthroplasty, 20(8), pp. 1060-1067.

[8] Edwards, M. L., 2000, "Below knee prosthetic socket designs and suspension systems," Phys. Med. Rehabil. Clin. N. Am., 11(3), pp. 585-593, vi.

[9] Incavo, S. J., Coughlin, K. M., Pappas, C., and Beynnon, B. D., 2003, "Anatomic rotational relationships of the proximal tibia, distal femur, and patella: implications for rotational alignment in total knee arthroplasty," J. Arthroplasty, 18(5), pp. 643-648.

[10] Hollister, A. M., Jatana, S., Singh, A. K., Sullivan, W. W., and Lupichuk, A. G., 1993, "The axes of rotation of the knee," Clin. Orth. Rel. Res., (290), pp. 259-268.

[11] Churchill, D. L., Incavo, S. J., Johnson, C. C., and Beynnon, B. D., 1998, "The transepicondylar axis approximates the optimal flexion axis of the knee," Clin. Orth. Rel. Res., (356), pp. 111-118.

[12] Roland, M. R., Hull, M. L., and Howell, S. M., 2010, "Virutal axis finder: a new method to determine the two kinematic axes of rotation for the tibio-femoral joint," J Biomech. Eng., (132).

[13] Woltring, H. J., 1994, “3-D attitude representation of human joints: a standardization proposal,” J Biomech. 27(12), pp. 1399-414.

[14] Roos, P., Hull, M., and Howell, S., 2004, “How cyclic loading affects the migration of radio-opaque markers attached to tendon grafts using a new method: A study using roentegen stereophotogrammetric analysis RSA,” J. Biomech., (126), pp. 62-69.

[15] Windolf, M., Gotzen, N., and Morlock, M., 2008, "Systematic accuracy and precision analysis of video motion capturing systems - exemplified on the Vicon-460 system," J. Biomech., 41(12), pp. 2776-2780.

TABLES

Table 2.1: Average errors in identifying the LR and FE axes of rotation with a mechanical validation versus a virtual validation for motion analysis. The virtual validations mimicked the mechanical validations with marker placement, rotational axis placement, and measurement error. Mechanical validations had an n of 5 and virtual validations had an n of 1000. The asterisks denote a significant difference between mechanical and virtual validation techniques (p=0.019).

	LR Axis				FE Axis			
	Orientation (deg)		Position (mm)		Orientation (deg)		Position (deg)	
	Mech.	Virtual	Mech.	Virtual	Mech.	Virtual	Mech.	Virtual
Bias	0.10	0.00	0.10	0.00	0.12	0.01	0.05	0.01
Precision	0.23	0.27	0.24*	0.78*	0.34	0.41	0.24	0.25
RMSE	0.25	0.27	0.26	0.78	0.36	0.41	0.25	0.25

Table 2.2: Average errors in identifying the LR and FE axes of rotation with a mechanical validation versus a virtual validation for RSA. The virtual validations mimicked the mechanical validations with marker placement, rotational axis placement, and measurement error. Mechanical validations had an n of 5 and virtual validations had an n of 1000.

	LR Axis				FE Axis			
	Orientation (deg)		Position (mm)		Orientation (deg)		Position (mm)	
	Mech.	Virtual	Mech.	Virtual	Mech.	Virtual	Mech.	Virtual
Bias	0.27	0.00	0.12	0.03	0.28	0.03	0.09	0.03
Precision	0.95	1.22	0.76	0.50	0.77	0.83	0.30	0.37
RMSE	0.98	1.22	0.77	0.50	0.82	0.83	0.32	0.37

FIGURES

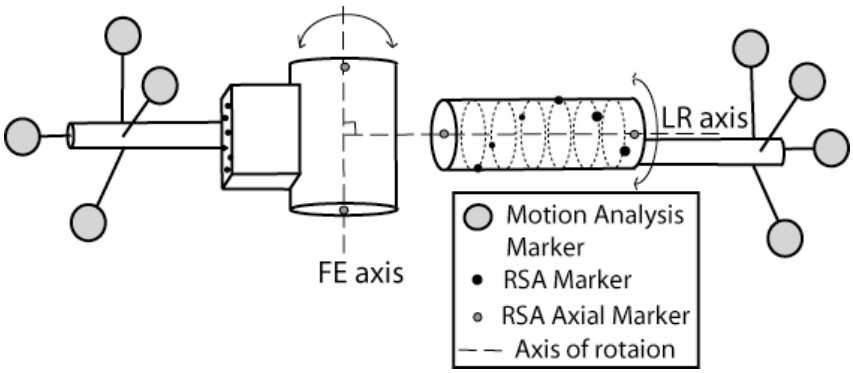

Figure 2.1: Diagram of the two orientation axis mechanism. The horizontal shaft simulated the FE axis of rotation and the vertical axis simulated the LR axis of rotation. The axes of rotation were fixed with respect to one another so that they were perpendicular and intersecting. Six 0.8 mm diameter tantalum RSA markers were fixed to both shafts and two 0.8 mm diameter tantalum RSA axial markers were fixed along the geometric axes to identify the axes of rotation with respect to the RSA markers. An array of four reflective motion analysis markers was fixed to each shaft. A coordinate measurement machine was used to measure centroids of the reflective markers and the geometric axes of the shafts to identify the axes of rotation with respect to the motion analysis markers.

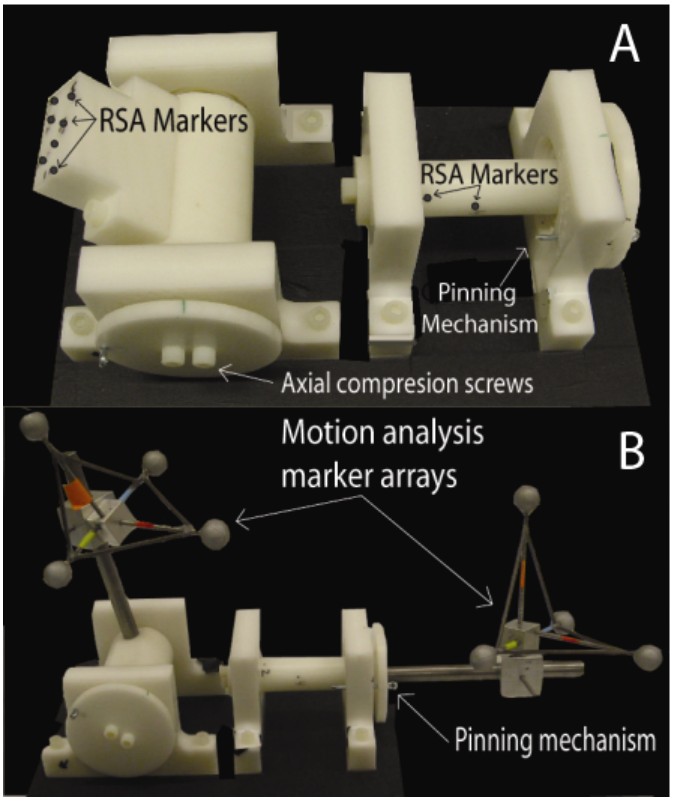

Figure 2.2: Photographs of the two orientation axis mechanism with RSA markers (A) and motion analysis markers (B). The shafts were rotated in 5° steps by rigidly pinning the large end disks to the pillow block by means of precision-machined holes placed in 5° steps along a 90° arc. The pillow blocks were mounted to a base plate to fix the orientation axes with respect to one another. The shafts rotated in ball bearings which were press fit into each pillow block. Axial compression along the inner race minimized off-axis motion.

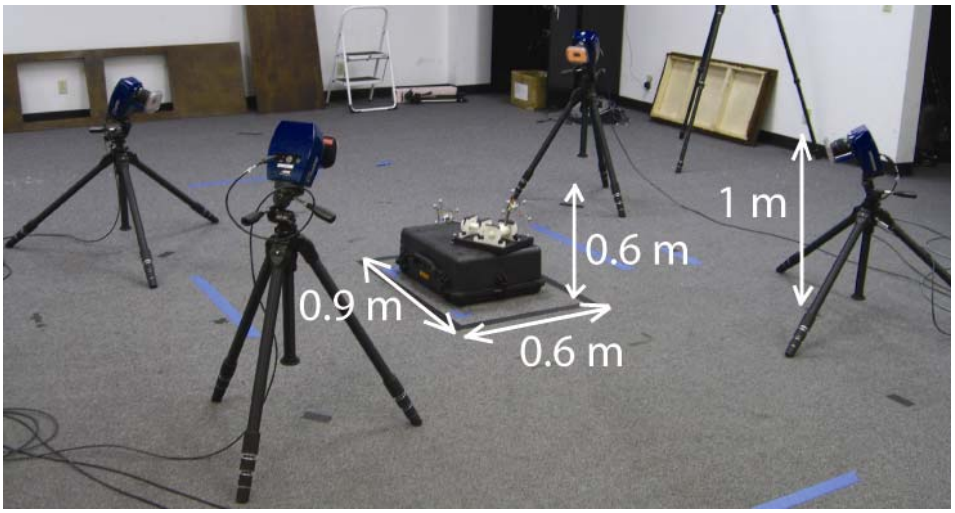

Figure 2.3: Photograph of the motion analysis set-up. The calibration volume was 0.6 x 0.9 x 0.6 m and the four Raptor 4 cameras (Motion Analysis Corp., Santa Rosa, CA) were positioned 1 to 1.3 m above the bottom of the calibrated volume in a 1.5 m arc around the center of the calibrated volume.

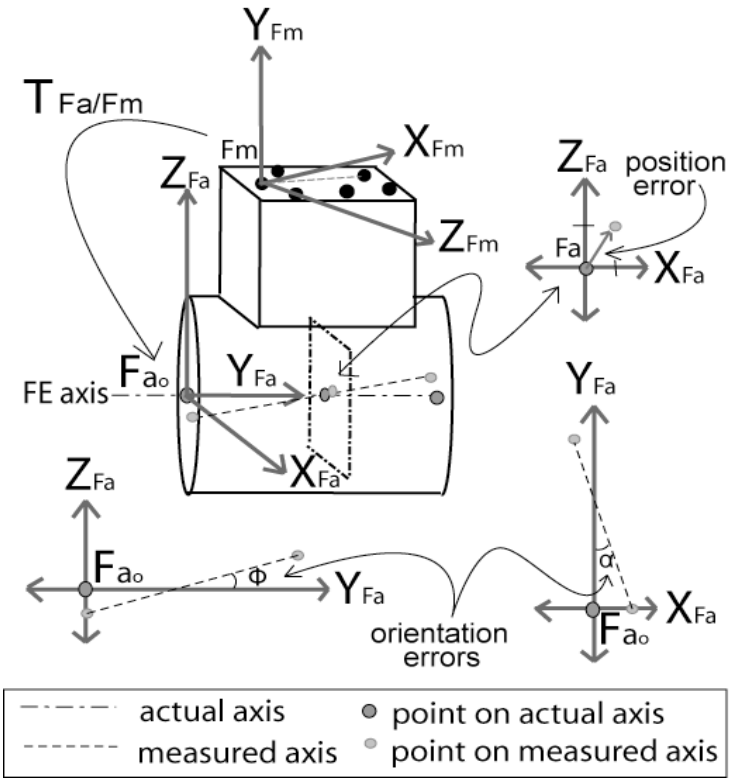

Figure 2.4: Diagram of the transformations used to perform the error analysis with the FE axis shaft and RSA markers. The marker coordinate system (F_m), which was defined by three markers fixed to the shaft, is transformed into an axial coordinate system (F_a) such that one axis is aligned with the actual axis of rotation ($T_{Fa/Fm}$). The position error was defined by the 2D position vector from the FE axis to the measured axis in a plane that was perpendicular to the actual axis and contained the minimum distance between the actual and measured axes. The orientation error was defined by two projection angles (ϕ and α) between the measured and actual axes onto the two perpendicular planes that were parallel to the FE axis and contained the origin of the axial coordinate system (Z_{Fa}-Y_{Fa} and Y_{Fa}-X_{Fa} planes).

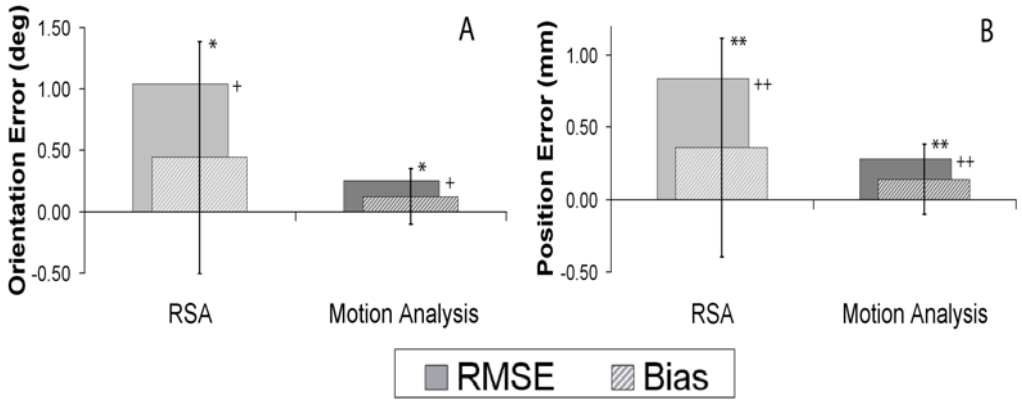

Figure 2.5: Bar chart comparing RSA and 3D video-based motion analysis as the measurement modality for the orientation (A) and position (B) RMSE, bias, and precision (error bars) for identifying the LR axis of rotation. There was a significant difference between precisions for the orientation (*p=0.008) and the position (p=0.024) errors and a significant difference between RMSE for the orientation (+ p=0.01) and position (++ p=0.03) errors.**

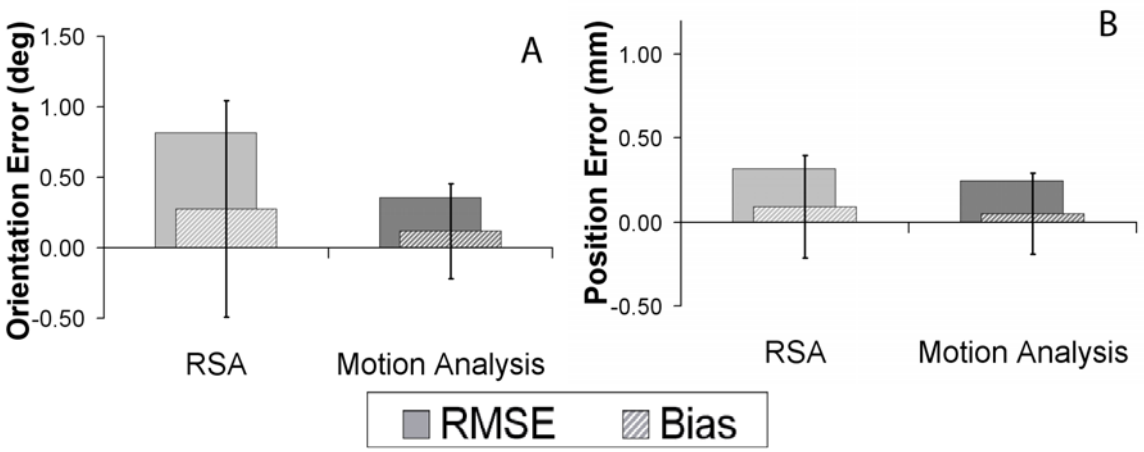

Figure 2.6: Bar chart comparing RSA and 3D video-based motion analysis as the measurement modality for the orientation (A) and position (B) RMSE, bias, and precision (error bars) for identifying the FE axis of rotation. There were no significant differences.